University of Tartu
Faculty of Science and Technology
Institute of Ecology and Earth Sciences
Department of Geography

Master's Thesis in Geoinformatics for Urbanized Society (30 ECTS)

Mapping Surface Urban Heat Islands and the influence of urbanization and heatwaves on urban climate through Local Climate Zones in Tallinn - 2014 and 2022

Author: Moritz Mühlbauer

Supervisor: Dr. Valentina Sagris

Tartu 2025

Abstrakt

Pinnalähedaste soojussaarte dünaamika linnas ja kuumalainete mõju kaardistamine kohaliku kliimavööndi kaardistamise kaudu Tallinnas aastatel - 2014 ja 2022

Käesolevas uurimistöös analüüsitakse linnastumist ja linnade pinnalähedase soojussaare intensiivsust (*Surface Urban Heat Island Intensity*, SUHII) Tallinnas aastatel 2014 – 2022, keskendudes kuumalaine ja tavatingimuste erinevustele. Linnastumist hinnati kohaliku kliimatsooni (*Local Climate Zone*, LCZ) kaardistamise kaudu, mis põhineb näidistega klassifitseerimisel (*supervised classification*) kasutades kaardiandmeid hoonete ja maakatte kohta ning Landsat 8 satelliitpilte. Satelliidilt mõõdetud maapinna temperatuuri (*Land Surface Temperature, LST*) andmeid kasutati temperatuuri mustrite ja SUHII hindamiseks. Tulemused näitavad linnastumise tihenemist Tallinna Kesklinnas ja selle ümbruses, ilma et oleks selgeid tõendeid valglinnastumise kohta Tallinna linna administratiivpiirides. SUHII oli kuumalainete ajal pidevalt kõrgem, eriti kompaktsetes, kõvakattega pinnaga piirkondades, samal ajal kui taimestatud ja vett läbi laskvad alad vähendasid liigset soojust. Vaatamata hoonestuse tihenemisele ei täheldatud SUHI ulatuse või intensiivsuse üldist suurenemist. Tulemused näitavad maakatte rolli olulisust soojushaavatavuses ja rõhutavad rohelise infrastruktuuri tähtsust kliimamuutustega kohanemisel. Edaspidistes uuringutes tuleks täpsustada referentskliimatsooni valikut ja laiendada ajalist ulatust, et suurendada SUHII hindamise täpsust.

Kohalikud kliimatsoonid, linnade pinnalähedased soojussaared, kuumalained, linnastumine, linnakliima, kaugseire, geoinfosüsteemid.

CERCS-kood: P510 – Füüsiline geograafia, geomorfoloogia, mullateadus, kartograafia, klimatoloogia; T181 – Kaugseire

Abstract

Mapping Surface Urban Heat Islands and the influence of urbanization and heatwaves on urban climate through Local Climate Zones in Tallinn – 2014 and 2022

This study analyses urbanization and Surface Urban Heat Island (SUHI) Intensity in Tallinn in 2014 and 2022, focusing on changes during heatwave and non-heatwave conditions. Urbanization was assessed through Local Climate Zone (LCZ) mapping based on supervised classification using building, land cover data, and Landsat 8 imagery. Satellite-derived Land Surface Temperature (LST) was used to evaluate thermal patterns and SUHI intensity. The results indicate urban densification in and around Kesklinn, with no clear evidence of urban sprawl within municipal boundaries. SUHI intensity was consistently higher during heatwaves, particularly in compact, impervious zones, while vegetated and pervious areas mitigated excess heat. Despite built-up densification, no overall increase in SUHI extent or intensity from 2014 to 2022 was observed. The findings underscore the role of land cover in thermal vulnerability and highlight the importance of green infrastructure in climate adaptation. Future studies should refine the methodology in the selection of the reference climate zone for SUHI/non-SUHI delineation and extend the temporal range to enhance the accuracy of SUHI intensity assessments.

Keywords: Local Climate Zones, Surface Urban Heat Islands, Heatwaves, Urbanization, Urban Climate, Remote Sensing, GIS.

CERCS code: P501 – Physical geography, goemorfology, pedology, cartography, climatology; T181 – Remote Sensing

List of abbreviations

LCZ	Local Climate Zones
UHI	Urban Heat Island
SUHI	Surface Urban Heat Island
LST	Land surface temperature
NDVI	Normalized Difference Vegetation Index
NDWI	Normalized Difference Water Index
NDBI	Normalized Difference Built-up Index
TIR	Thermal infrared
SWIR	Shortwave infrared

Table of Contents

1 Introduction

Since 1950, the global urban population has increased significantly, from 751 million to 4.5 billion in 2024, surpassing 50% of the total population (United Nations, 2024). Projections estimate that by 2050, approximately 68% of the world's population will reside in urban areas (Brozovsky et al., 2021). This rapid urbanization has intensified challenges associated with climate change, including the rise in extreme weather events.

Urban areas develop distinct climatic conditions, characterized by elevated surface and air temperatures, increased exposure to pollutants, reduced wind flow, and lower solar radiation levels (Brozovsky et al., 2021). These altered environmental conditions contribute to abrupt temperature fluctuations and intensify thermal stress, primarily driven by the replacement of vegetated surfaces with impervious built-up infrastructure (Aslam & Rana, 2022). One of the most prominent manifestations of this transformation is the Urban Heat Island (UHI) effect, defined as the measurable temperature difference between urbanized areas and their rural surroundings (Debbage & Shepherd, 2015).

Heatwaves represent another intensifying climatic hazard and are closely linked to UHIs. Their interaction tends to amplify both the intensity and spatial extent of urban heat anomalies, posing additional risks to urban populations (Liu et al., 2018). These dynamics are not exclusive to megacities; in Estonia, urban areas such as Tallinn are increasingly experiencing UHI effects comparable to those of larger Western and Central European cities (Sagris & Sepp, 2017).

Against this background, this study investigates the influence of heatwaves and urbanization on UHIs measured with land surface temperature (LST), so-called Surface Urban Heat Islands (SUHIs) in Tallinn, comparing 2014 and 2022. The temporal comparison of SUHI patterns provides an opportunity to explore how urbanization contributes to the severity and spatial extent of urban heat stress.

To analyse SUHI intensity and magnitude, this study adopts the Local Climate Zone (LCZ) framework. The LCZ classification, based on "information-rich intra-urban classes" (Demuzere et al., 2021), offers a robust methodology for delineating diverse urban land covers and quantifying their climatic impacts.

Heatwave and non-heatwave days were selected based on meteorological maximum daily air temperature records. Supervised classification with a Random Forest algorithm was used to

generate the LCZ maps. The training area was obtained by combining Landsat 8 satellite imagery with building and land cover vector data. The satellite imagery was retrieved using the Python API Geemap, streamlining images through Google Earth Engine (GEE). Processing was performed using a combination of QGIS and Python scripts within a Jupyter Notebook environment.

LCZ training areas for 2014 and 2022 were submitted to a multi-temporal LCZ mapping script to evaluate urban densification and sprawl over time. Based on the resulting LCZ classifications, thermal LCZ maps, also referred to as SUHI maps, were generated using LST data for both years under heatwave and non-heatwave conditions. SUHI intensity was defined as the mean LST difference between each LCZ and a reference zone, while SUHI magnitude was quantified as the total area exceeding this baseline.

By combining vector data, LCZ classification, satellite-derived LST, and extreme temperature events, this study aims to deepen the understanding of how urban morphology and heatwaves interact to shape SUHI dynamics in Tallinn. The findings provide important insights for urban planning and climate adaptation in northern European cities.

2 Urbanization and heatwaves: Impacts on the urban climate

2.1 Mapping urban morphology: Local Climate Zones

2.1.1 Concept of Local Climate Zones

To standardise urban research and make the assessment of urban climate more differentiated and precise, the concept of LCZs was developed to improve the division between urban and rural sites (Stewart & Oke, 2012). The name has been considered appropriate due to the classes being defined at a local scale, with a climatic basis and a zonal representation (Stewart & Oke, 2012).

The classification into LCZs aims to ease the acquisition of site metadata and the quantification of the UHI magnitude regardless of the city examined. A central novelty of this approach is the recognition that the terms urban and rural cannot sufficiently explain complex and diverse urban environments and surroundings in the necessary richness of detail (Stewart & Oke, 2012). In doing this, the concept does not replace the terms urban and rural as the main differentiation but rather refines them into more accurate subdivisions. The urban-rural division, predominantly based on the number of buildings and population, is expanded to LCZs as “regions of

uniform surface cover, structure, material, and human activity that span hundreds of meters to several kilometers in horizontal scale" (Stewart & Oke, 2012).

Each LCZ is assigned a distinct named class based on one or more defining surface characteristics, primarily determined by the height/packing of roughness elements or the prevalent land cover (Stewart & Oke, 2012). Those characteristics are often referred to as urban morphology or the physical form of settlement (Aslam & Rana, 2022). The LCZ concept divides urban landscapes into 17 standard classes (**Figure 1**). The built-up classes 1-10 are delineated by surface cover (entirely/partially paved or soil), building height (low-, mid-, or high-rise), and density (sparse, open, or compact) (Stewart & Oke, 2012). The land cover or natural classes A-G are differentiated by vegetation density and height (dense trees, scattered trees, bush and scrub or low plants) and type of surface cover (bare rock/paved or bare soil/sand) (Stewart & Oke, 2012).

Analyzing changes over time helps to understand how building height, density, and the ecological space have transformed over the years. The coverage ratio, building type, and functionalities affect the climatic conditions. Each block can show different structures that have an influence on the local urban climate (Aslam & Rana, 2022). These physical attributes are quantifiable and universally applicable, devoid of specificity concerning location or time. The final goal of dividing urban areas into LCZs is understanding the relationship between the built environment and local climate (Aslam & Rana, 2022).

Previous research has already used LCZs to analyze urban climate, heat stress, and urbanization. A Croatian study linked LST and LCZs to investigate urban climate in 9 Croatian cities (Žgela et al., 2024). In Saudi Arabia, LCZs were deployed to analyze the thermal characteristics of Riyadh city (Alghamdi et al., 2021). In Brno, HUMIDEX gauged human heat exposure across LCZs was assessed (Geletič et al., 2018). In Shenzhen, LCZs were used to investigate thermal comfort (Liu et al., 2018). Finally, Khoshnoodmotlagh et al. (2021) detected urban morphology and linked these with LST for Tehran Metropolis in Iran.

Built types	Definition	Land cover types	Definition
1. Compact high-rise 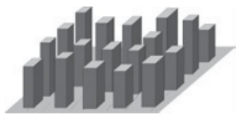	Dense mix of tall buildings to tens of stories. Few or no trees. Land cover mostly paved. Concrete, steel, stone, and glass construction materials.	A. Dense trees 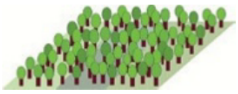	Heavily wooded landscape of deciduous and/or evergreen trees. Land cover mostly pervious (low plants). Zone function is natural forest, tree cultivation, or urban park.
2. Compact midrise 	Dense mix of midrise buildings (3–9 stories). Few or no trees. Land cover mostly paved. Stone, brick, tile, and concrete construction materials.	B. Scattered trees 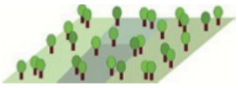	Lightly wooded landscape of deciduous and/or evergreen trees. Land cover mostly pervious (low plants). Zone function is natural forest, tree cultivation, or urban park.
3. Compact low-rise 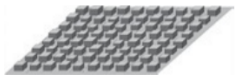	Dense mix of low-rise buildings (1–3 stories). Few or no trees. Land cover mostly paved. Stone, brick, tile, and concrete construction materials.	C. Bush, scrub 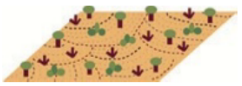	Open arrangement of bushes, shrubs, and short, woody trees. Land cover mostly pervious (bare soil or sand). Zone function is natural scrubland or agriculture.
4. Open high-rise 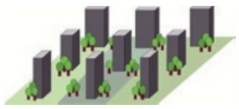	Open arrangement of tall buildings to tens of stories. Abundance of pervious land cover (low plants, scattered trees). Concrete, steel, stone, and glass construction materials.	D. Low plants 	Featureless landscape of grass or herbaceous plants/crops. Few or no trees. Zone function is natural grassland, agriculture, or urban park.
5. Open midrise 	Open arrangement of midrise buildings (3–9 stories). Abundance of pervious land cover (low plants, scattered trees). Concrete, steel, stone, and glass construction materials.	E. Bare rock or paved 	Featureless landscape of rock or paved cover. Few or no trees or plants. Zone function is natural desert (rock) or urban transportation.
6. Open low-rise 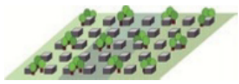	Open arrangement of low-rise buildings (1–3 stories). Abundance of pervious land cover (low plants, scattered trees). Wood, brick, stone, tile, and concrete construction materials.	F. Bare soil or sand 	Featureless landscape of soil or sand cover. Few or no trees or plants. Zone function is natural desert or agriculture.
7. Lightweight low-rise 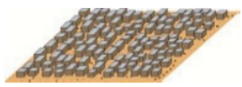	Dense mix of single-story buildings. Few or no trees. Land cover mostly hard-packed. Lightweight construction materials (e.g., wood, thatch, corrugated metal).	G. Water 	Large, open water bodies such as seas and lakes, or small bodies such as rivers, reservoirs, and lagoons.
8. Large low-rise 	Open arrangement of large low-rise buildings (1–3 stories). Few or no trees. Land cover mostly paved. Steel, concrete, metal, and stone construction materials.	**VARIABLE LAND COVER PROPERTIES**	
		Variable or ephemeral land cover properties that change significantly with synoptic weather patterns, agricultural practices, and/or seasonal cycles.	
9. Sparsely built 	Sparse arrangement of small or medium-sized buildings in a natural setting. Abundance of pervious land cover (low plants, scattered trees).	*b. bare trees*	Leafless deciduous trees (e.g., winter). Increased sky view factor. Reduced albedo.
		s. snow cover	Snow cover >10 cm in depth. Low admittance. High albedo.
10. Heavy industry 	Low-rise and midrise industrial structures (towers, tanks, stacks). Few or no trees. Land cover mostly paved or hard-packed. Metal, steel, and concrete construction materials.	*d. dry ground*	Parched soil. Low admittance. Large Bowen ratio. Increased albedo.
		w. wet ground	Waterlogged soil. High admittance. Small Bowen ratio. Reduced albedo.

Figure 1: Types and definitions of LCZs (Stewart & Oke, 2012)

2.1.2 Local Climate Zone characteristics and classification approaches

The LCZ classification scheme was organized in a simplified way along two primary axes: building height, representing the most significant aspect of urban structure, and surface permeability, reflecting the key characteristic of urban fabric and land cover (Bechtel et al., 2015).

Figure 2 displays a methodological outline for approximating the highly differentiated classification characteristics of LCZs through remote sensing indicators. The arrows are used to suggest possible wavelength bands and features that could aid in discrimination.

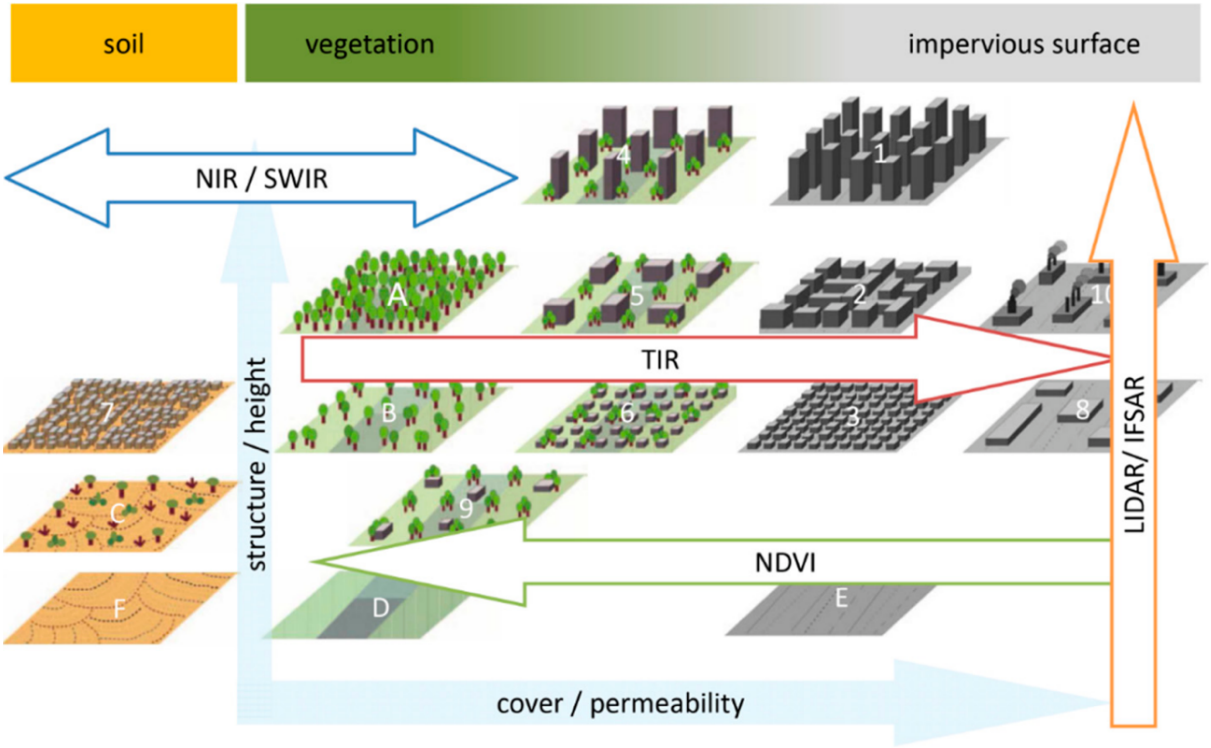

Figure 2: Observable characteristics to distinguish LCZs from remote sensing data (Bechtel et al., 2015)

Generally, it can be stated that not all surface climatic properties are easily captured through remote sensing. Observing from space remains challenging, and analysing urban structure requires very high-resolution data, which is typically not freely available (Bechtel et al., 2015). Nevertheless, Landsat imagery has been widely used, given its extensive archive of moderate-resolution multispectral data spanning over four decades, which is accessible free of charge through the United States Geological Survey (USGS) (Bechtel et al., 2015).

A main distinction between vegetation and soil or sand can be achieved using near and shortwave infrared (SWIR) (Bechtel et al., 2015). This aids in identifying LCZs 7, C, and F. To further narrow down vegetation into LCZs A-D, the Normalized Vegetation Index (NDVI)

serves as a solid measure, since it enables the distinction between dense and sparse vegetation (USGS, 2018).

For pervious and artificial zones, thermal infrared (TIR) can be used, since these exhibit higher values in this spectrum (Bechtel et al., 2015). Additionally, the Normalized Difference Built-Up Index (NDBI), being calculated using the TIR band, proved to be a powerful tool in detecting built-up areas (Zha et al., 2003). These generally enable the localization of built-up LCZs 1-10 as well as LCZ E.

The further subdivision of built LCZs into sparse, open, and compact, as well as low-, mid- and high-rise, follows along building height and density. This step remains the most challenging due to limited data availability (Bechtel et al., 2015). There are global datasets from the Shuttle Radar Topography Mission and the ASTER Global Digital Elevation Map, but those only offer limited surface models, which are too coarse and noisy for distinguishing between highly differentiated LCZs (Bechtel et al., 2015).

If available, it is advantageous to incorporate vector or raster data, ideally on building level. These allow an accurate distinction between different degrees of building density and height. Additionally, when combining detailed building data with land cover, these datasets facilitate the identification of mixed zones, which are the most difficult to identify due to their mixed properties of buildings and vegetation in between.

2.1.3 Methodological and practical limitations

However, the LCZ system, while useful, oversimplifies urban and rural environments by reducing the landscape to basic elements like buildings, roads, vegetation, soil, rock, and water, organized into 17 distinct patterns (Stewart & Oke, 2012). Yet, the uniformity depicted within each LCZ is rarely found outside of deliberately planned or meticulously managed areas. Despite this, the 17 patterns should be recognizable across most urban areas and adaptable to local characteristics. They can be seen as the "best practice" regarding combining continuous phenomena such as temperature and climate with the topology of urban space (Stewart & Oke, 2012).

Furthermore, the LCZ characteristics are not ideally suited for supervised classification, since there is a considerable degree of redundancy and overlap among individual LCZ characteristics (Bechtel et al., 2015). This suggests that while multiple features are necessary for effective classification, not all of them contribute equally to distinguishing between zones (Bechtel et al.,

2015). Additionally, some of these features cannot be directly observed using Earth observation data, making it necessary to identify alternative data sources. However, these are mostly not publicly available and difficult and expensive to collect, especially for building properties (Demuzere et al., 2020).

2.2 Measuring heatwaves in Estonia

Heatwave definitions vary widely across studies, making it difficult to compare results. Some studies use metrics based on daily maximum and minimum air temperatures, while others employ more complex, multi-measurement indices that consider intensity, frequency, duration, and spatial extent (Perkins & Alexander, 2013).

The study and measurement of extreme temperatures, particularly heatwaves, present significant challenges due to their rarity and the high-quality, daily data required for accurate calculations (Perkins, 2015). Frich et al. (2002) addressed some of these issues by proposing ten climate indicators, five of which pertain to temperature extremes. These indicators were designed to be robust, widely applicable, and derivable from available observations. This work was pivotal in standardizing the measurement of temperature extremes.

A framework proposed by Perkins and Alexander (2013) seeks to standardize heatwave measurement by using three baselines (daily minimum and maximum temperatures and the excess heat factor) and a consistent threshold (the calendar-day 90th percentile).

Previous research has already combined LCZs and heatwaves in quantifying the effects of urban spatial characteristics on outdoor thermal comfort using the LCZ concept (Liu et al., 2018). In the Baltic context, Jaagus et al. (2024) investigated long-term changes in heatwave parameters in the eastern Baltic region. In Estonia, Sagris and Sepp (2017) assessed the UHI effect and its impact on human health employing Landsat 8 data. In their study, they used the 98^{th} percentile of 27 °C of the maximum daily air temperature to measure heatwaves in Estonia.

2.3 Urban climate in response to urbanization and heatwaves

2.3.1 Surface urban heat islands and land surface temperature

UHIs describe a longer duration and higher maximum air temperature in cities than in the outer suburbs (Aslam & Rana, 2022). "Local urban heat island intensities are also an alternative term to determine the heat concentrations and help determine the effects of local urbanization" (Aslam & Rana, 2022). Approaches to quantify UHI typically fall into two categories: direct

measurement of air temperature or remote sensing of Land Surface Temperature (LST), also named "skin temperature of the surface" (Sagris & Sepp, 2017). Concluding, SUHIs are a specific subtype of UHIs that can be measured using LST (Alexander, 2020).

SUHIs are prevalent across urban areas of all sizes, irrespective of climatic conditions (Brozovsky et al., 2021). The SUHI phenomenon is not exclusive to megacities; northern European cities exhibit heightened vulnerability compared to their Southern counterparts (Brozovsky et al., 2021).

2.3.2 Estimating thermal characteristics of Local Climate Zones

LCZs exhibit distinct vertical temperature patterns, particularly noticeable over arid and flat terrains during tranquil, cloudless nights (Stewart & Oke, 2012). These thermal conditions are shaped by the characteristics of surface cover types such as urban environments, natural ecosystems, and agricultural areas (Debbage & Shepherd, 2015).

Air temperature, especially LST, the main variable to measure SUHIs, is used in LCZ mapping to analyze thermal stress and identify hotspots in compact urban areas (Vaidya et al., 2024). Land surface conditions, analyzed with land use and cover, and surface morphology, determined by building density, height, and sprawl, influence LST, which in turn is used to identify heat hotspots (Stewart & Oke, 2012). Then again, those shifts in urban microclimates can be well captured by LCZ and subsequently assemble SUHI models. "LCZs can help to produce the heat map of the city so that thermal conditions can be monitored adequately" (Aslam & Rana, 2022).

To substantially quantify the SUHI magnitude, it is common to use temperature differences of LCZs. These provide information about the "changing urban landscape and its properties for proper urban renewal and planning" (Aslam & Rana, 2022). It's a suitable method for studying urban forms and climates at a local scale (Aslam & Rana, 2022).

2.3.3 Urbanization's impact on amplifying Surface Urban Heat Islands during heatwaves

Intensified urban structures cause higher temperatures and "thermal stress" compared to less developed rural sites (Aslam & Rana, 2022). Dense, high-rise, and low-vegetation urban areas contribute significantly to the formation and intensification of SUHIs (Stewart & Oke, 2012). Heatwaves further elevate LST, with highly urbanized zones responding more strongly than less built-up, vegetated environments such as forests, grasslands, or parks (Emmanuel &

Loconsole, 2015). As a result, urbanization increases SUHI intensity, especially under extreme heat conditions. **Figure 3** illustrates how compact, built-up morphology raises both LST and SUHI intensity, whereas open or low-rise areas have a mitigating effect. Similarly, vegetated land cover reduces, while paved or sealed surfaces increase LST and SUHIs. Heatwaves exacerbate these effects, raising overall temperatures. These dynamics can be effectively captured using the LCZ framework.

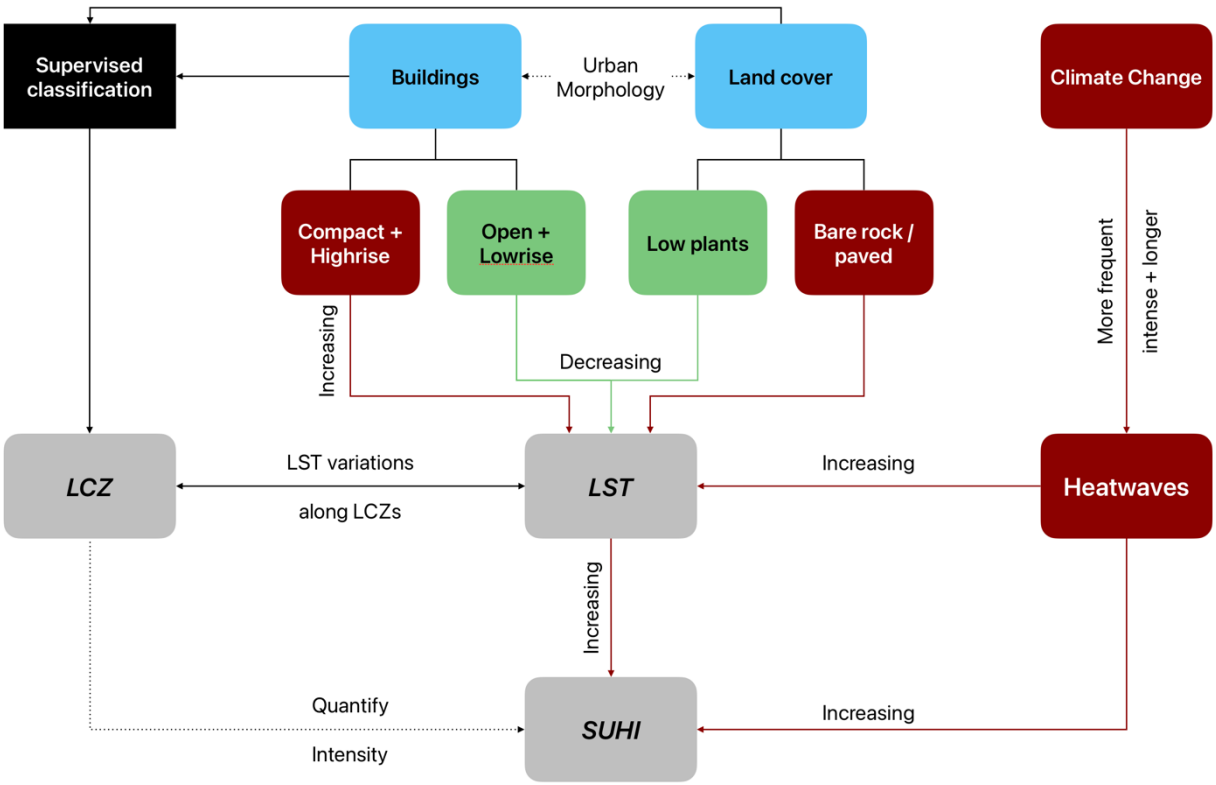

Figure 3: Impact of urbanization on amplifying SUHIs during heatwave periods and measuring through LCZs

2.4 Research gaps, questions and objective

The LCZ classification scheme has proven to be an established and effective framework for analysing urbanization and urban climate. Previous research on the effects of heatwaves on human health in Tallinn has highlighted a growing concern, pointing to the urgent need for a better understanding of how the built environment responds to extreme temperature events. SUHI intensity serves as a widely accepted metric for capturing urban–rural temperature

contrasts, offering valuable insights into how cities, in particular, heat up during periods of extreme weather.

This study aims to address the following research gaps:

1. A further temporal comparison of urban climate data in Tallinn across multiple years
2. The classification of Tallinn into LCZs using a multi-temporal approach
3. The integration of heatwave data with SUHI analysis through LCZ classification

These gaps give rise to the following research questions:

RQ1: Which districts in Tallinn experienced changes in the built environment, such as densification or urban sprawl, between 2014 and 2022?

RQ2: How does urban morphology influence the intensity of SUHIs in Tallinn?

RQ3: To what extent has urbanization in Tallinn between 2014 and 2022 influenced the intensity and magnitude of SUHIs?

RQ4: What is the effect of heatwaves on SUHI intensity in Tallinn?

The objective of this study is to evaluate how changes in the built environment between 2014 and 2022 have influenced the intensity and extent of SUHIs in Tallinn, and to assess the additional impact of heatwaves on urban thermal conditions. By applying the LCZ framework in combination with remote sensing-based LST and heatwave data, this study aims to quantify patterns of urban densification, determine their contribution to SUHI development, and identify spatial hotspots of thermal stress. Ultimately, the study seeks to support evidence-based urban climate adaptation by pinpointing vulnerable zones and highlighting the role of urban form and land cover in mitigating heat-related risks.

3 Data and methods

3.1 Study area: Tallinn municipality

This study investigates urbanization and SUHIs in the municipality of Tallinn in Estonia. **Figure 4** displays the Tallinn municipality and its districts and subdistricts. The latter are used to localize the investigated phenomena more precisely.

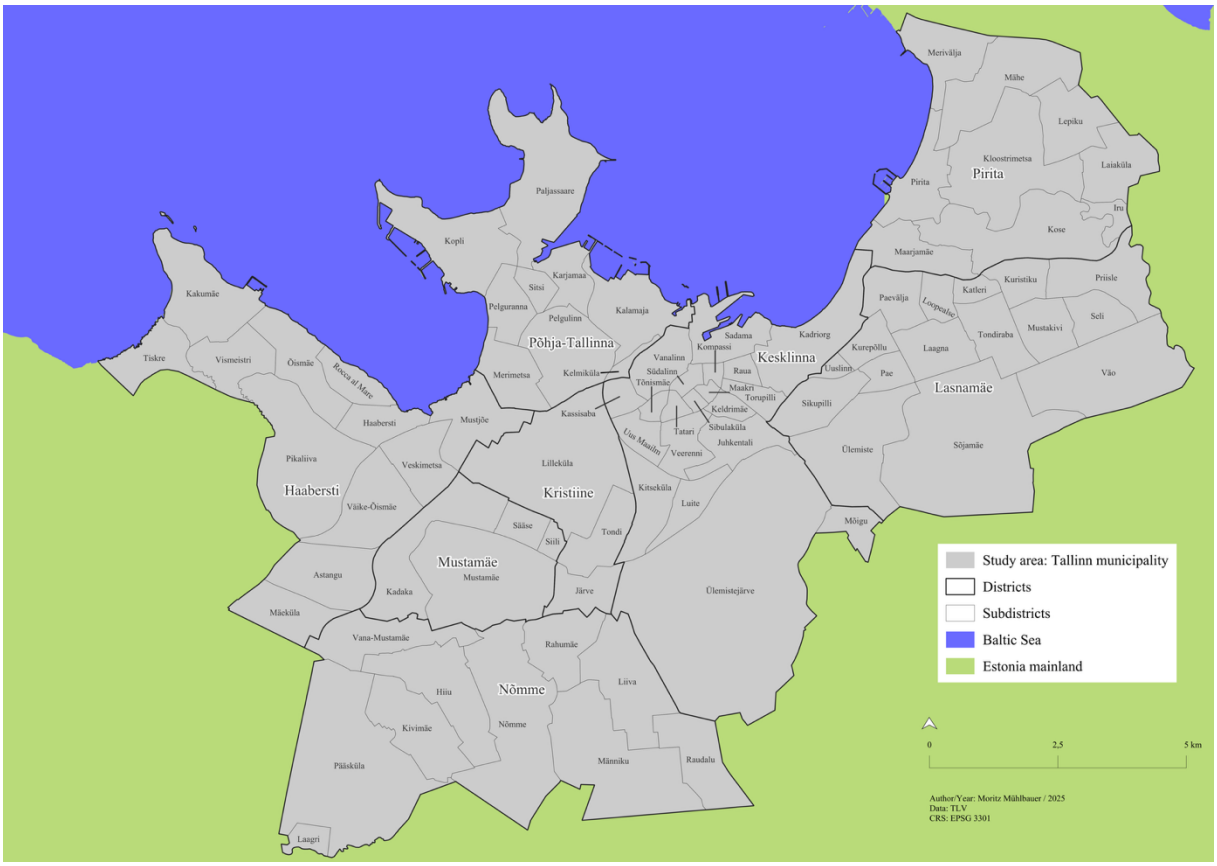

Figure 4: Study area Tallinn municipality and its districts and subdistricts

3.2 Workflow for mapping Local Climate Zones in Tallinn

The author developed a customized workflow to pre-identify the LCZ-specific training area to support the supervised classification into LCZs by combining Landsat 8 satellite images and building and land cover vector data (**Figure 5**). Like this, LCZ maps representing the urban morphology of Tallinn in 2014 and 2022 could be created to further analyse urbanization trends and estimate the Surface Urban Heat Island intensity for heatwave and non-heatwave days.

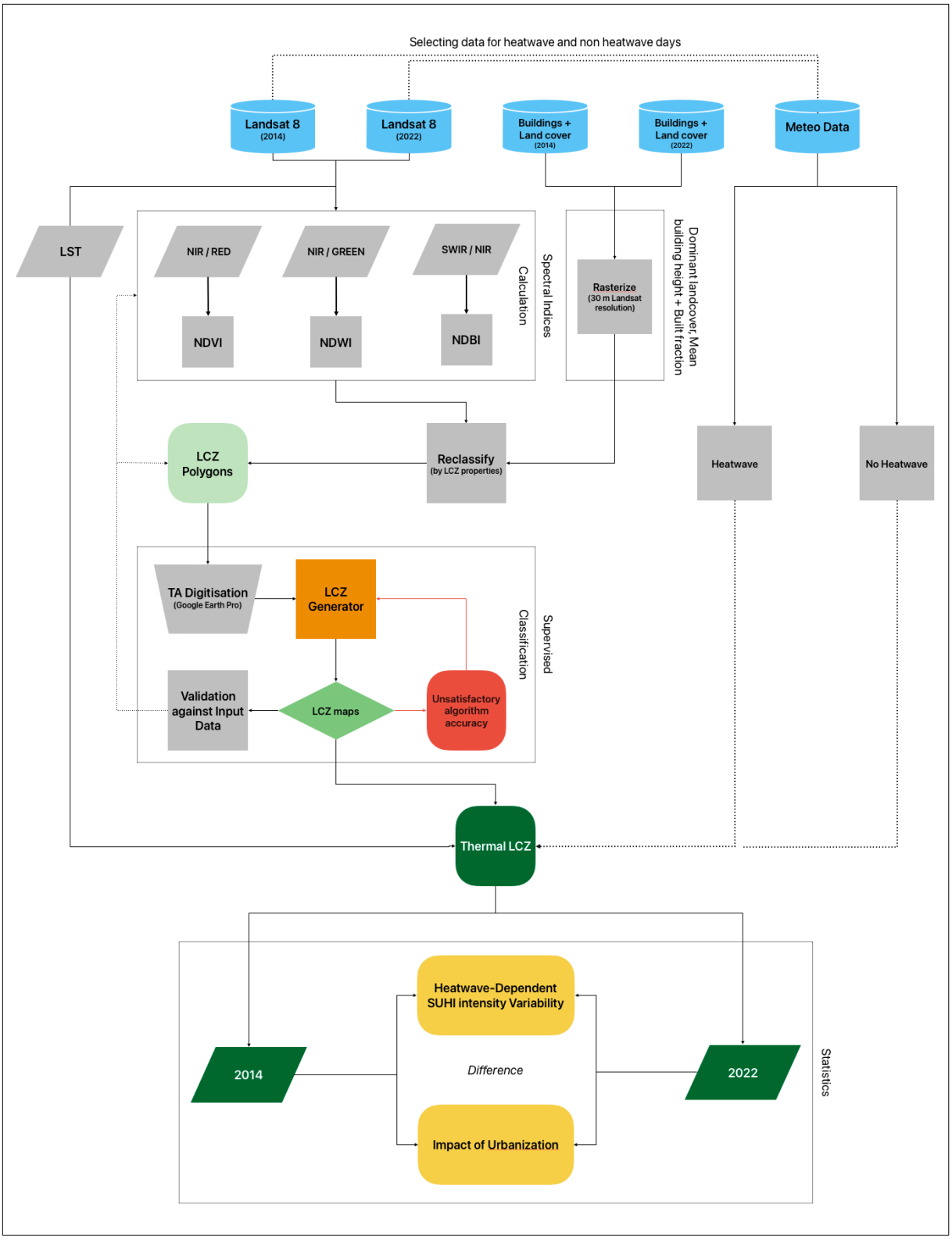

Figure 5: Methodological workflow for measuring urbanization and SUHI intensity by extracting LCZs through supervised classification via the integrated mapping of Landsat 8 satellite imagery, land cover, and building vector data in Tallinn for 2014 and 2022

3.3 Heatwave identification

The heatwave periods from 2014 to 2022 were identified based on the definition of heatwaves used by Sagris and Sepp (2017) for the Estonian climate. The raw, daily maximum air temperature was retrieved from the Estonian Environment Agency (EEA, n.d.) using a workflow previously established by Dr. Valentina Saagris in Sagris and Sepp (2017). The data was queried in JSON format from a URL based on the input parameters year, start and end month, and county and weather station name. Next, the data were normalized and converted to a data frame. The final data acquisition step was parsing the date column to date-time object of day of the year format and dropping all columns besides the date and daily temperature.

The heatwave periods of three consecutive days exceeding the temperature threshold of 27 °C were computed. First, a subset of air temperatures higher than 27 °C was created. Second, a rolling window over 3 days was computed over the subset and summed on the fly. As a result, a new column with the count of consecutive threshold-exceeding days was created. The minimum periods parameter was set to 1 to retrieve values for the first and second rows as well, since those did not form a three-day period yet. Thirdly, a new column for heatwave labeling was created and set to False by default.

Fourth and finally, a conditional statement checks if the rolling sum is higher than or equal to 3; if so, a heatwave is detected. Since the rolling window operation only assigns a value to the last value of the group, in this case, the end of a heatwave, the heatwave labeling was set to True backward until the beginning of the heatwave. The start of a heatwave, when going backward from its end, is indicated by a value set to False by default in the heatwave label column.

3.4 Integrated mapping of satellite, land cover, and building data

3.4.1 Prerequisites for automated Local Climate Zone identification

The bottleneck regarding classification accuracy of the LCZ maps is the training area digitization, which is referred to as a task for Local Urban Experts (Bechtel et al., 2015). Since the author has no Estonian background or expert knowledge about the study area, a systematic method to select training area polygons was developed. To automatically classify LCZs, specific physical and structural properties of the landscape must be identified. When these properties are accurately mapped and integrated, they can be used to train a supervised Random Forest classifier, enabling the automatic classification and mapping of LCZs within the dataset. In doing so, a modified threshold classification based on USGS (n.d.) for spectral indices and

building and land cover data based on Stewart and Oke (2012) (Annex 1) was created to pre-identify homogeneous zones before digitizing them (**Table 1**).

Table 1: LCZs and their properties by indicator for reclassification of land cover, building data, and spectral indices

Classes	LCZ	Land cover*	Built fraction (%)*	Building height (m)*	NDVI**	NDBI**
Built	1	Artifical surface without vegetation *(raster_code = 2)*	41 - 100 *(compact)*	> 25 *(highrise)*	-1 - 0.1	0.6 - 1
	2			10 - 25 *(midrise)*		
	3			2 - 9 *(lowrise)*		
	4	Artifical surface with vegetation *(raster_code = 1)*	20 - 40 *(open)*	> 25	0.2 - 0.5	0.2 - 0.5
	5			10 - 25		
	6			2 - 9		
	7	Artifical surface without vegetation	60 - 90 *(lightweight)*	2 - 4 *(lightweight lowrise)*	-1 - 0.1	0.6 - 1
	8		30 - 50 *(large)*	2 - 9		
	9	Artifical surface with vegetation	0 - 19 *(sparse)*		0.2 - 0.5	0.2 - 0.5
	10	Artifical surface without vegetation	20 - 40 *(open)*	5 - 15 *(heavy industry)*	-1 - 0.1	0.6 - 1
Natural	A	Natural surface with vegetation *(raster_code = 3)*	< 10	0	0.6 - 1	-1 - 0.1
	B					
	C					
	D	Natural surface without vegetation *(raster_code = 4)*			0.2 - 0.5	0.2 - 0.5
	E	Transportation *(raster_code = 6)*			-1 - 0.1	0.6 - 1
	F	Natural surface without vegetation				
	G	Water *(raster_code = 5)*			**NDWI** control	-

Data: * = Tallinn City Government (TLV), ** = USGS

Classification thresholds: *modified from Steward and Oke (2021), **= USGS

3.4.2 Dominant land cover, mean building height and built fraction computation

Landcover and building vector data were derived from the Tallinn City Government (TLV, n.d.) database, the attribute information was in Estonian. Additionally, land cover and building types were encoded by an integer type-id column. The datasets were translated from Estonian to English in cooperation with Dr. Valentina Sagris, and the decoding information from type-ids to actual types was obtained from the data provider. After translation and decoding, a raster code was assigned to land cover and building types, facilitating type distinction and aggregation. Annex 2 contains the tables used for translation, decoding, and aggregation for land cover and building types.

Next, the land cover datasets were assessed for quality and completeness. Significant gaps were identified and subsequently filled using the following approach. First, a polygon of the land-cover layer extent was computed. Second, the gaps were extracted as separate multi-part features. Third, every gap was obtained as a separate single-part feature polygon. Fourth, the area

of every single-part gap was calculated to distinguish between very small slivers and result-influencing gaps. A gap area of 350 m2 (half of the area of one 30x30 m grid cell) was judged as result-influencing. The gaps were merged back to the land cover and filled using aerial orthophotography of the respective year.

The same quality control was conducted for the building datasets. It became apparent that the building data for both years contained missing building height values. The missing heights were estimated from the number of stories. First, all rows with missing story and height values were dropped because no height estimation could be performed. Second, all buildings with 0 height and stories were dropped because the buildings did not seem to exist. Thirdly, the mean story height per building equal to or higher than 1 story was calculated with formula 1:

$$(1)\ mean\ story\ height = \frac{building\ height}{story\ amount}$$

The mean of all the buildings' 1-story heights was used as a threshold to estimate the missing height values. Following Dr. Valentina Sagris's proposal, the building height was estimated according to formula 3, if a building had 0 stories:

$$(3)\ estimated\ height = story\ amount + 1\ story\ threshold$$

And according to formula 4, if a building had one story or more:

$$(4)\ estimated\ height = story\ amount * 1\ story\ threshold$$

Lastly, buildings lower than 2 m were excluded from the dataset to comply with the minimum building height mentioned in the LCZ classification schema.

After translation, decoding, and cleaning, the aggregation of the vector datasets in a 30x30 m grid was performed to align land cover and buildings with Landsat satellite imagery in raster format and coarsen the resolution to the LCZ scale. The vectors were aggregated using a hexagonal grid (30 m width and height) to the extent of Landsat 8 satellite images (to ensure alignment).

To compute spatial metrics per grid cell, a common procedure was followed: the grid was intersected with the relevant spatial layer (land cover or buildings), grouped by the unique grid

cell ID and a relevant attribute, and aggregated values were calculated on the fly. The resulting data frames were then merged back to the spatial grid, retaining only matching IDs.

For dominant land cover, the intersected grid–land cover data was grouped by grid cell ID and raster code. The land cover type with the largest intersected area per grid cell was identified and assigned as the dominant type.

For the mean building height, the grid–building intersection was grouped by grid cell ID and building height. The mean height per cell was calculated, rounded to whole integers, and merged with the spatial grid containing only intersecting buildings.

For the built fraction, the total building area within each grid cell was summed and divided by the cell area (900 m^2) to calculate the built fraction in percent. This value was rounded to whole integers and merged back into the spatial grid.

3.4.3 Satellite image selection, rescaling, and spectral indices calculation

This author developed a workflow for selecting Landsat 8 images, especially for heatwave-sensitive LCZ mapping. The selected acquisition dates of the satellite images for heatwave days correspond to the heatwave periods, identified through air maximum daily air temperature. The images were selected based on low cloud cover and full coverage of the study area (Annex 3).

For visual inspection, collections containing year-specific satellite images were used. The images and their acquisition dates were added to an interactive map extent and checked for study area coverage and cloud cover. After visual inspection, 4 satellite images for 2014 were selected (**Figure 6**). The acquisition time is in UTC.

1. 2014-05-22 09:29:09: First non-heatwave image
2. 2014-05-22 09:29:33: Second non-heatwave image
3. 2014-07-25 09:29:32: First heatwave image
4. 2014-07-25 09:29:56: Second heatwave image

The two satellite images captured on the same day were merged into a mosaic composite, with overlapping areas averaged per pixel. This approach was appropriate given the nearly identical acquisition times and ensured complete spatial coverage. For 2022, a non-heatwave mosaic

could not be created owing to limited availability. The following 3 images were selected (**Figure 6**):

1. 2022-05-21 09:23:49: Non-heatwave image
2. 2022-08-16 09:30:11: First heatwave image
3. 2022-08-16 09:30:35: Second heatwave image

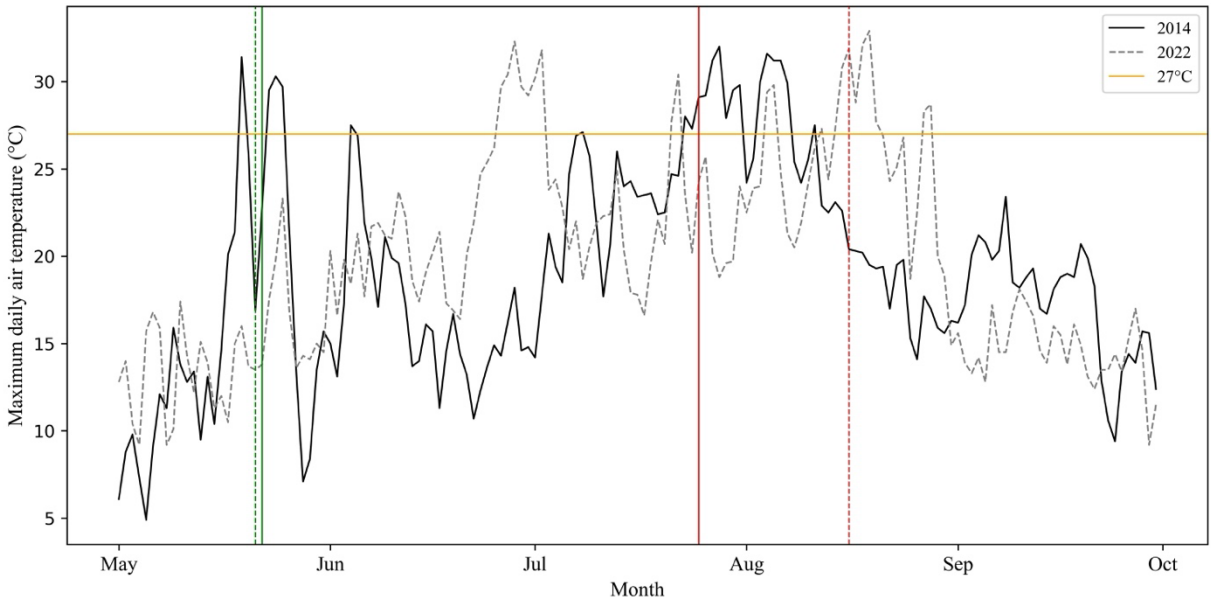

Figure 6: Maximum daily air temperature in 2014 and 2022 and selected satellite images acquisition dates: green straight line - no heatwave image 2014, green dashed line - no heatwave image 2022, red straight line - heatwave image 2014, red dashed line heatwave image 2022

All images throughout the acquisition dates were acquired almost at the same time of the day, making these perfect for a comparative analysis. Moreover, the heatwave images of both years stem from the beginning of a heatwave period, ensuring more comparable conditions and reducing temperature bias from prolonged heat exposure. Furthermore, all images were captured at around 12:30 pm, Estonian time, when, according to Stewart and Oke (2012), the maximum SUHI intensity can be observed.

After selection, the images were radiometrically rescaled. Landsat 8 Level 2 (L2) images are classified as analysis-ready data, meaning they are atmospherically and geometrically corrected (USGS, 2024). The top-of-atmosphere (TOA) reflectance is pre-scaled to surface reflectance (SR) and geographically aligned. Nevertheless, the data is provided in digital numbers (DN),

and those must be converted to physical reflectance or temperature units (TU) using scaling factors (USGS, 2024).

Optical bands were rescaled from surface reflectance (DNs ranging from 0 to 1) to physical reflectance (PR) using formula 5:

$$(5)\ PR = SR * 0.0000275 - 0.2$$

Thermal bands containing LST were rescaled to °C with formula 6:

$$(6)\ TU = SR * 0.00341802 - 124.15$$

After radiometric rescaling, the spectral indices could be calculated. The Normalized Difference Vegetation Index (NDVI) has been widely utilized as a spectral index for quantifying vegetation greenness, serving as a proxy for vegetation density and an indicator of plant physiological status. It is conventionally derived from the normalized difference between surface reflectance in the red (R) and near-infrared (NIR) spectral bands (USGS, 2018):

$$(7)\ NDVI = \frac{(NIR - R)}{(NIR + R)}$$

The Normalized Difference Water Index (NDWI) is a remote sensing-derived metric designed to detect and monitor water bodies. It is calculated using the reflectance values of the green (G) and NIR spectral bands, as follows (USGS, n.d.):

$$(8)\ NDWI = \frac{(G - NIR)}{(G + NIR)}$$

The Normalized Difference Built-up Index (NDBI) was specifically designed to identify and map built-up areas using satellite imagery (Zha et al., 2003). It is calculated using the SWIR and NIR reflectance values:

$$(9)\ NDBI = \frac{(SWIR - NIR)}{(SWIR + NIR)}$$

The index leverages the spectral characteristics of urban surfaces, which typically exhibit higher reflectance in the SWIR region than in the NIR region. As a result, built-up areas are generally associated with higher NDBI values, while vegetation and water bodies tend to produce negative values. The method has proven to be effective in distinguishing urban environments from

other land cover types, particularly in Landsat imagery (Zha et al., 2003). Compare Annex 4 and the code documentation in the reference section for maps of the spectral indices and LST.

3.5 Extracting Local Climate Zones from combined mapping

3.5.1 Multi-temporal Local Climate Zone mapping with supervised classification

Demuzere et al. (2021) have launched a web application for LCZ mapping that classifies training areas (provided as KML/KMZ files) into Gaussian-filtered LCZ maps using Earth observation data. The training areas are used as input to a supervised Random Forest classifier implemented in Google Earth Engine. The full code access is provided in a GitHub repository created by Demuzere (2022), which was successfully tested for Canadian cities by Demuzere et al. (2020). This methodology was utilized for multi-temporal climate zone mapping in Tallinn. By adjusting the input parameters, year-specific LCZ maps can be created, allowing a temporal comparison between 2014 and 2022.

All input features are derived within a time window of one year before and after the census year, and restricted to the months between May and October (Julian days 120 to 240) to minimize the influence of snow cover (Demuzere, 2022). With the exception of the minimum and maximum NDVI and the maximum NDWI, all other spectral bands were processed as median composites at a spatial resolution of 30 meters.

In June 2024, the USGS completed its migration from Landsat Collection 1 to Collection 2 (USGS, 2024). This transition introduced changes to asset identifiers, band naming conventions, scaling factors, and quality assurance (QA) layers, which affected the compatibility of existing scripts that rely on Earth Engine data. As a result, the methodology required several updates to function correctly with the new Collection 2 datasets.

To address these changes, the script was modified to incorporate the updated asset IDs for Landsat 5, 7, and 8; revised band names; adjusted rescaling factors for both optical and thermal bands; and improved QA masking procedures. These updates were implemented based on current documentation and best practices related to Collection 2 data handling.

The author contacted M. Demuzere on this topic and presented his modifications. M. Demuzere agreed to work collaboratively with the author on updating the present workflow of multi-

temporal climate zone mapping. Finally, the author's modifications were integrated into the default multi-temporal LCZ mapping package.

3.5.2 Training area selection

To distinguish between natural and artificial environments in Tallinn, aggregated land cover classes (Annex 5) were combined with spectral indices. NDVI was extracted only for land cover types classified as natural surfaces, both with and without vegetation, while NDBI was applied to artificial surfaces, both vegetated and non-vegetated, as well as transportation areas (Annex 6). Prior to this, the interoperability of the land cover and building datasets was assessed, confirming that buildings occur exclusively within artificial surface classes. Based on this initial classification, it was reasonable to expect LCZs 1–10 to fall within artificial environments and LCZs A–G within natural ones. Water was excluded from this analysis due to its distorting effect on both indices (producing consistently low values).

This fundamental distinction between natural and artificial environments serves as a basis for refining LCZ subtypes. To support this process, a field visit to Tallinn was conducted on 27 March 2025, during which training area selections were reviewed and verified on site.

The artificial environment was further classified into built-up LCZs 1–10 by integrating mean building height and built fraction. Mean building height per grid cell, derived from aggregated building data, was used to distinguish low-, mid-, and high-rise structures (Annex 7). Built fraction per grid cell, also based on building data, was used to identify varying degrees of density, including sparse, large, open, and compact built areas (Annex 8). By combining both height and density parameters, specific LCZs (e.g., compact high-rise) were assigned accordingly.

To further refine the classification, the land cover class artificial surface with vegetation was used to differentiate compact zones (LCZs 1–3) from open, sparse, or large zones (LCZs 4–10). The land cover class transportation provided additional support in identifying LCZ 8 (large low-rise) and LCZ 10 (heavy industry), given its extensive paved surface characteristics.

The classification of built LCZs was further supported by NDBI. In areas where no buildings were present but a high NDBI response was observed, the classification LCZ E (bare rock or paved) was assigned to reflect the presence of impervious artificial surfaces.

As this study did not have access to vegetation density, height, or health data, the refined classification of the natural environment into LCZs A–G was based on land cover, NDVI,

orthophotos, and field observations. Water bodies were reliably delineated using the dedicated land cover class "water" and further refined with NDWI.

LCZ A (dense trees), LCZ B (scattered trees), and LCZ D (low plants) were initially identified using the dominant land cover type, natural surface with vegetation. This classification was then refined by combining the land cover information with NDVI values, enabling the differentiation of vegetation densities. LCZ C (bush and scrub) and LCZ F (bare soil/sand) were identified using the land cover class natural surface without vegetation and further evaluated with NDVI to verify vegetation absence or sparse cover.

3.6 Measuring urbanization with Local Climate Zones

LCZs support the assessment of urbanization by distinguishing between artificial and natural land cover. In this study, built-up types, as well as paved and bare soil/sand zones, are classified as urban. While not strictly built-up, paved surfaces are strong indicators of urbanization due to their impervious and artificial nature. The bare soil/sand class was included to capture transitional areas, such as construction sites or zones under demolition, reflecting dynamic changes in urban morphology.

Based on this classification, the extent of urban LCZs serves as an indicator of urban sprawl. To quantify this, the area of each urban LCZ was calculated by multiplying the number of pixels by the pixel area (900 m^2). This allowed for a direct comparison of urban LCZ coverage between 2014 and 2022. The total area of all urban LCZs combined was used as the overall metric to assess urban sprawl over the study period.

Since LCZ classes differentiate urban form by density, ranging from sparse, to open, to compact, urban densification was assessed by analyzing transitions of urban LCZs into more compact classes. This was achieved by a transition map created by encoding LCZ changes as unique two-digit values, where the first two digits represent the LCZ class in 2014 and the last two digits represent the corresponding class in 2022 (e.g., a transition from LCZ 1 to LCZ 5 is encoded as 105). Grid cells that did not exhibit a class change or fell outside the valid class

subset were excluded from further analysis by masking them out of the resulting transition raster.

This approach allowed for the identification and quantification of all valid LCZ transitions, enabling a focused assessment of spatial urban form changes over time.

3.7 Estimating and comparing Surface Urban Heat Island intensity

To provide an initial statistical foundation for estimating SUHI intensity, LST distributions were analyzed across LCZs using box plots. These plots summarize the variability and central tendencies of LST per LCZ, offering insights into the thermal behavior of different urban forms and surface types. The statistical metrics used, median, standard deviation, and maximum daily air temperature, serve as key indicators for interpreting thermal differences between LCZs.

The median LST was chosen as a stable measure of central tendency, reducing the influence of outliers commonly present in remotely sensed temperature data (Žgela et al., 2024). This enables consistent comparison of LST across LCZs and years, which is critical for identifying zones with elevated surface temperatures. The standard deviation quantifies internal variability within each LCZ, reflecting how consistently or variably a given zone responds thermally. A low standard deviation suggests uniform surface heating, while a high standard deviation may indicate heterogeneous land cover or mixed material properties.

The maximum daily air temperature was included to relate surface conditions to atmospheric background temperatures and to support contextual interpretation of LST patterns. This statistical approach establishes a baseline understanding of urban–rural thermal contrasts and prepares the groundwork for spatial SUHI intensity maps, which visualize the intensity and distribution of urban heat in greater detail.

SUHI intensity is calculated as the difference between the mean LST of each LCZ and that of the reference zone, LCZ D (Stewart & Oke, 2012). LCZ D is selected as the reference due to its minimal urban characteristics and is assumed to exhibit the lowest LST values among the urban-related classes, making it suitable for representing non-built-up environments (Demuzere et al., 2021). As LCZ D still belongs to the broader urban fabric, this approach refines the SUHI

concept by framing it as an intra-urban indicator of the influence of built structures on the urban thermal environment, rather than a simple urban–rural comparison (Stewart & Oke, 2012).

Accordingly, the SUHI intensity for each LCZ is computed relative to the mean LST of LCZ D. This enables the creation of SUHI intensity maps that visualize the thermal contribution of different LCZs and reveal spatial patterns of urban heating.

4 Results

4.1 Local Climate Zones in Tallinn - 2014 and 2022

4.1.1 Classification and spatial patterns

This section presents the multi-temporal LCZ classification results and spatial patterns for 2014 and 2022 through LCZ maps (**Figure 7**). The LCZ maps were produced with an overall accuracy of ~0.7 for 2014 and 2022 (Annex 9), comfortably surpassing the threshold of 0.5 defined by Bechtel et al. (2015).

The districts are described by their LCZ characteristics. If necessary, the subdistricts will be mentioned to provide a more detailed localization. Further, the LCZs are used to quantify the urban sprawl (4.1.2) and densification (4.1.3) as the two main sub-processes of urbanization.

The LCZs 3 (compact low-rise) and 7 (lightweight low-rise) were not detected in the study area. LCZ 6 (open low-rise) and 9 (sparsely built) were almost equally present in the residential areas of Nõmme, Haabersti, and Pirita. Finally, the author decided, based on the mean built fraction of these districts (lower than the threshold for open zones), to classify them as sparsely built.

The Tallinn municipality can generally be divided into the dense, urbanized center in the Kesklinn district, sparse residential areas to the East and West in the districts Nõmme, Pirita, and Haabersti, and open residential or large commercial areas in Mustamäe, Põhja-Tallinna, and Lasnamäe. In the following, the intra-district distribution of LCZs is elaborated in more detail.

Starting in 2014, Kesklinn is the most urbanized district of Tallinn, characterized primarily by open mid-rise and compact mid- to high-rise areas. The historic center, Vanalinn, features compact midrise structures, while a dense high-rise zone extends through Südalinn, Maakri, Kompassi, and Sadama to the northeast. North of this urban core lies the public passenger ferry harbor, classified as paved and large low-rise due to its vast parking areas and docks. In the

east, Kadriorg Park introduces green space with scattered trees, bordered by compact midrise development along the shoreline.

Lasnamäe, located northeast of Kesklinn, is a mixed-use district with a highly diverse LCZ profile. The southern part features the paved airport area across Ülemiste and Sõjamäe, transitioning into a dominant large low-rise zone of commercial and industrial facilities. Scattered compact midrise pockets appear where building heights exceed the low-rise threshold. The northern half is characterized by open high-rise zones with Soviet-era residential blocks and interspersed green spaces. At the northeastern edge, near the city limits, lies a broad soil and sand zone, while the southern border with Pirita is marked by a wide stretch of bush and scrub, representing unpopulated natural wasteland. Together, these elements highlight Lasnamäe's complex blend of transport infrastructure, industry, open housing, and undeveloped land.

Pirita is one of Tallinn’s least urbanized districts, characterized primarily by natural and sparsely built zones. Its center is dominated by bush, scrub, low vegetation, and dense to scattered trees, encompassing the Pirita River protected area, Tallinn Botanical Garden, and surrounding recreation forest. The subdistricts of Merivälja, Mähe, Lepiku, Kose, and Marjamäe form a broad sparsely built zone along the district’s edges. On the northern coastline, a sailing harbor classified as industrial marks one of the few developed areas.

Located in the western part of Tallinn, Nõmme shares similar LCZ characteristics with Pirita, being predominantly sparsely built with scattered patches of dense trees and low vegetation. A large low-rise zone runs along Pärnu mnt and Männiku tee, complemented by a small open to compact mid-rise area in the southwest, representing an industrial storage or distribution center. Overall, Nõmme is defined by its sparsely built residential character with limited industrial development.

Combining the districts of Mustamäe and Kristiine due to their similar LCZ coverage, those encompass open mid and high-rise residential and a wide-ranging large low-rise zone. Therefore, both districts show a use between residential and industrial/commercial domains.

2014

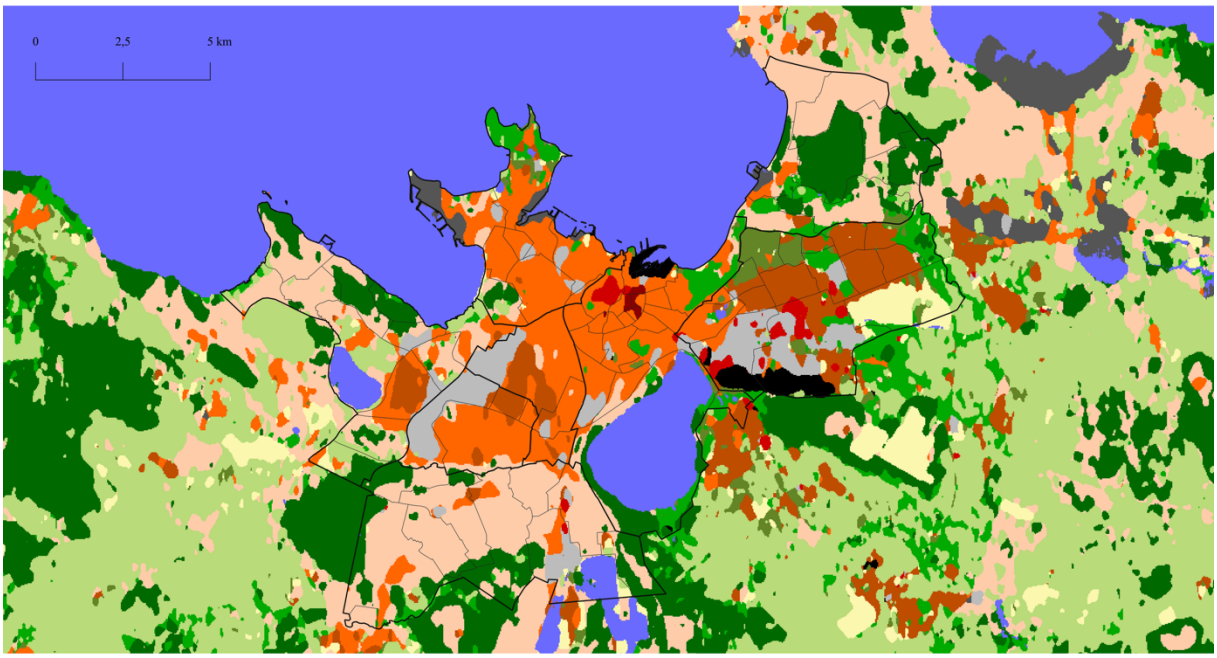

2022

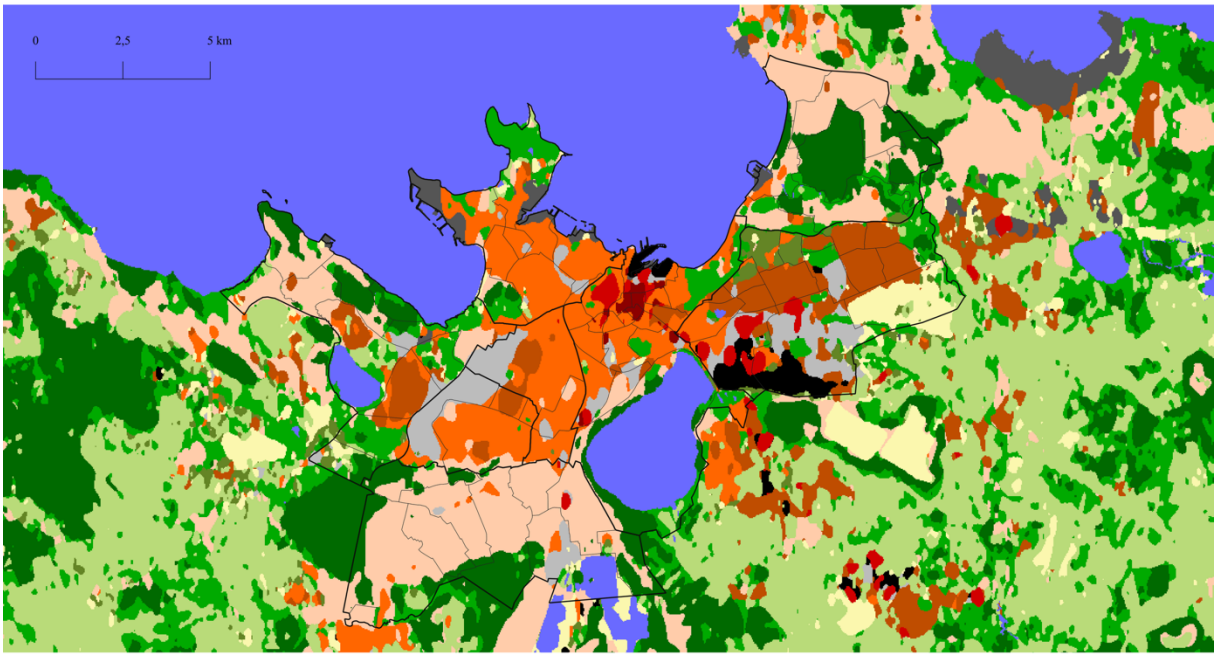

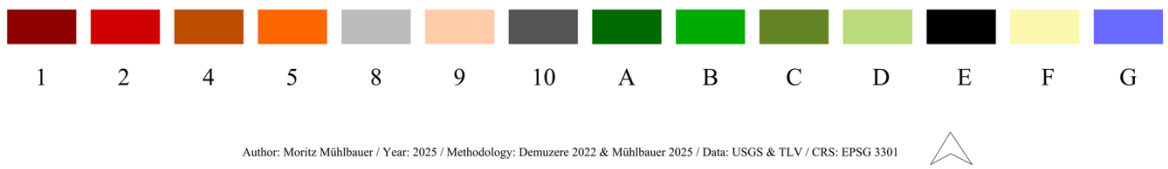

Author: Moritz Mühlbauer / Year: 2025 / Methodology: Demuzere 2022 & Mühlbauer 2025 / Data: USGS & TLV / CRS: EPSG 3301

Figure 7: LCZs of 2014 and 2022, LCZ key: 1 - Compact high-rise, 2 – Compact mid-rise, 4 – Open high-rise, 5 – Open mid-rise, 8 – Large low-rise, 9 – Sparsely built, 10 – Heavy Industry, A – Dense trees, B – Scattered trees, C – Bush and scrub, D – Low plants, E – Paved or bare rock, F – Bare soil or sand, G - Water

Haabersti, located northwest of Mustamäe, features a mix of LCZs with a predominance of sparse and open midrise zones. The Väike-Õismäe subdistrict stands out with open mid- and high-rise developments. In contrast, the northern subdistricts—Tiskre, Kakumäe, Vismeistri, Õismäe, and Rocca al Mare—are mostly sparsely built or covered by dense tree vegetation. The southeastern areas of Veskimetsa and Mustjõe include open midrise and large low-rise zones. Overall, Haabersti is primarily defined by sparse and mid-rise development, with a notable high-rise concentration in Väike-Õismäe.

Põhja-Tallinn, forming the northern headland of the city, is primarily an open midrise residential district. Industry zones dominate the eastern and western coastlines, where industrial ports and plants are located. The central area includes large low-rise patches, while smaller, sparsely built zones appear near the western port. Scattered tree coverage marks the northern tip. Overall, Põhja-Tallinn combines residential midrise development with industrial coastal infrastructure.

In 2022, Kesklinn, the most urbanized district in Tallinn, has seen continued densification, with a clear shift toward more compact development. While open midrise remains dominant, compact mid- and high-rise zones have expanded notably. Former paved areas near the passenger port—such as Rotermann and Porto Franco—have been transformed into compact midrise zones. The compact high-rise core has grown, with additional patches forming to the south and near the paved zone, paralleled by an expanded large low-rise area in front of the port. New open high-rise developments have appeared southwest of the high-rise core along Tartu mnt and Keskturg, while Veerenni street has seen the emergence of low-rise commercial and midrise residential areas. The open midrise zone along Kadriorg Park has also extended eastward. Overall, Kesklinn's LCZs reflect a clear trend toward increased compactness and urban density.

Lasnamäe changed in a similar manner. The paved zone representing the airport and the compact midrise patches around grew. The large low-rise zone grew in the East due to new commercial centers and got replaced by compact mid and open high-rise in the West (Ülemiste Technopolis area and T1 shopping center). Parts of the bush/scrub wasteland got replaced by open mid-rise residential development.

4.1.2 Urban sprawl through urban Local Climate Zone area changes

Changes in urban LCZ areas were analyzed to quantify urban sprawl between 2014 and 2022 (**Figure 8**).

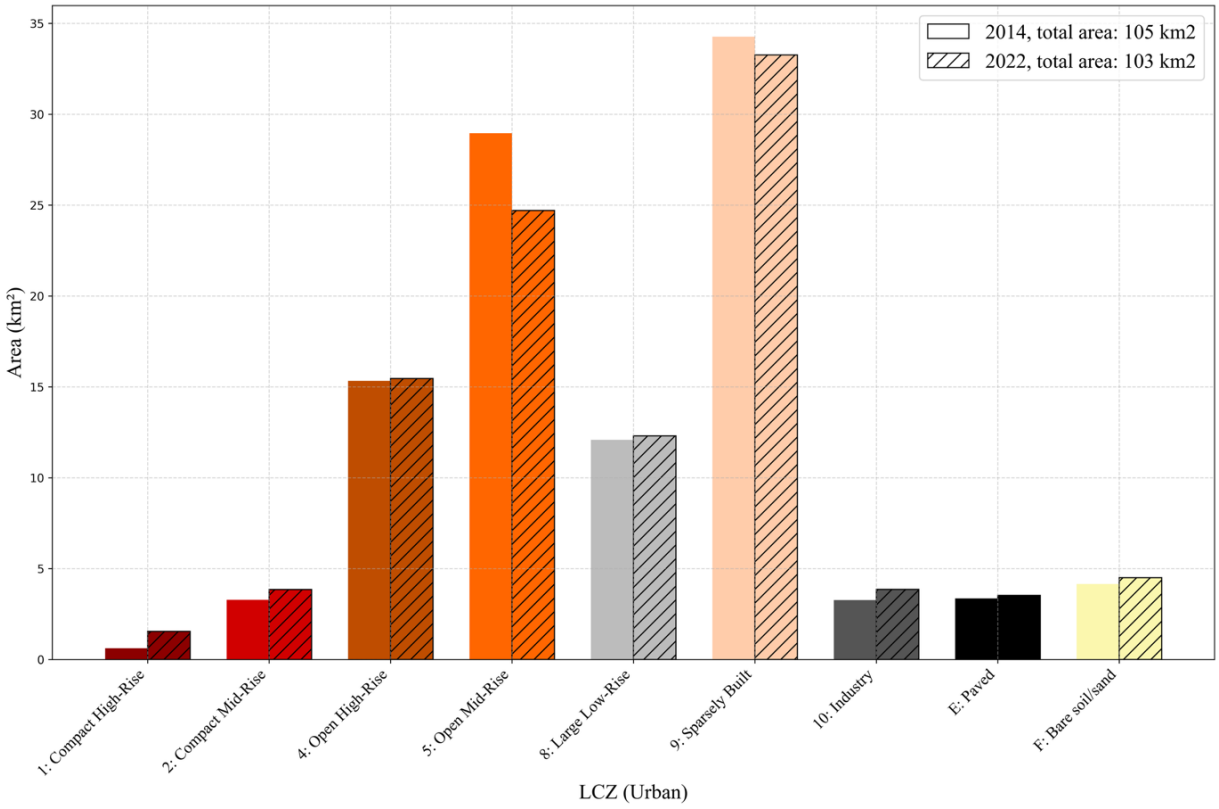

Figure 8: Area of urban LCZs in 2014 and 2022

The most notable increase in absolute area occurred in compact high-rise and compact mid-rise zones, which gained approximately 0.9 km² and 1.0 km², respectively, suggesting densification in the central urban core.

In contrast, open mid-rise areas showed a substantial reduction of over 4 km², marking the most significant decrease among all categories. Sparsely built areas also declined by about 1 km², indicating a broader shift away from more scattered or less dense developments.

Open high-rise, large low-rise, industry, and bare soil/sand categories remained relatively stable, with minor increases of less than 0.4 km² each.

Finally, while all LCZs, except the open mid-rise and sparsely built zone, which dropped significantly, increased in area, the total urban LCZ area decreased by 2 km2 from 2014 to 2022.

Following, no considerable uptake of rural by urban LCZ classes can be seen, and therefore, an urban sprawl within the Tallinn municipality borders could not be detected.

4.1.3 Urban densification through urban Local Climate Zone transitions

Since in 4.2.1 there was no urban sprawl found, but an increase in compact mid and high-rise zones was detected, this chapter analyzes urban densification as an intra-urban transition of LCZs to either LCZ 1 or 2 (**Figure 9**). Due to the non-existent urban sprawl, no transitions from urban to natural zones are examined. This analysis generalizes the transition of non-compact but built-up LCZs (sparse, open, large, and industry) and non-built-up but urban LCZs (paved and bare soil/sand) as an indicator of urban densification. Industry does not represent a typical urban zone, but parts of the passenger port were classified as such in 2022.

It becomes evident that transitions to compact zones from the other urban LCZs are more frequent than the reverse. In numbers, 3.23 km2 of urban LCZs transitioned into one of the compact zones, while 0.79 km2 (without large low-rise) converted into less dense zones. A notable aspect of density decrease is the transition from compact to large low-rise, which took place to an extent of 0.1 km2.

The urban center of Kesklinn experienced the majority of densification overall, and the strongest growth of compact high-rise. In Lasnamäe, the compact mid-rise grew predominantly, while southeastern patches indicate the extension of large low-rise areas. Kristiine and Mustamäe show less intensive densification with compact patches growing in the northwest and the large low-rise zone expanding to the South. Concluding, the net flow of urban LCZs towards more compact areas is + 2.44 km2, indicating urban densification mainly in and clustered around Kesklinn.

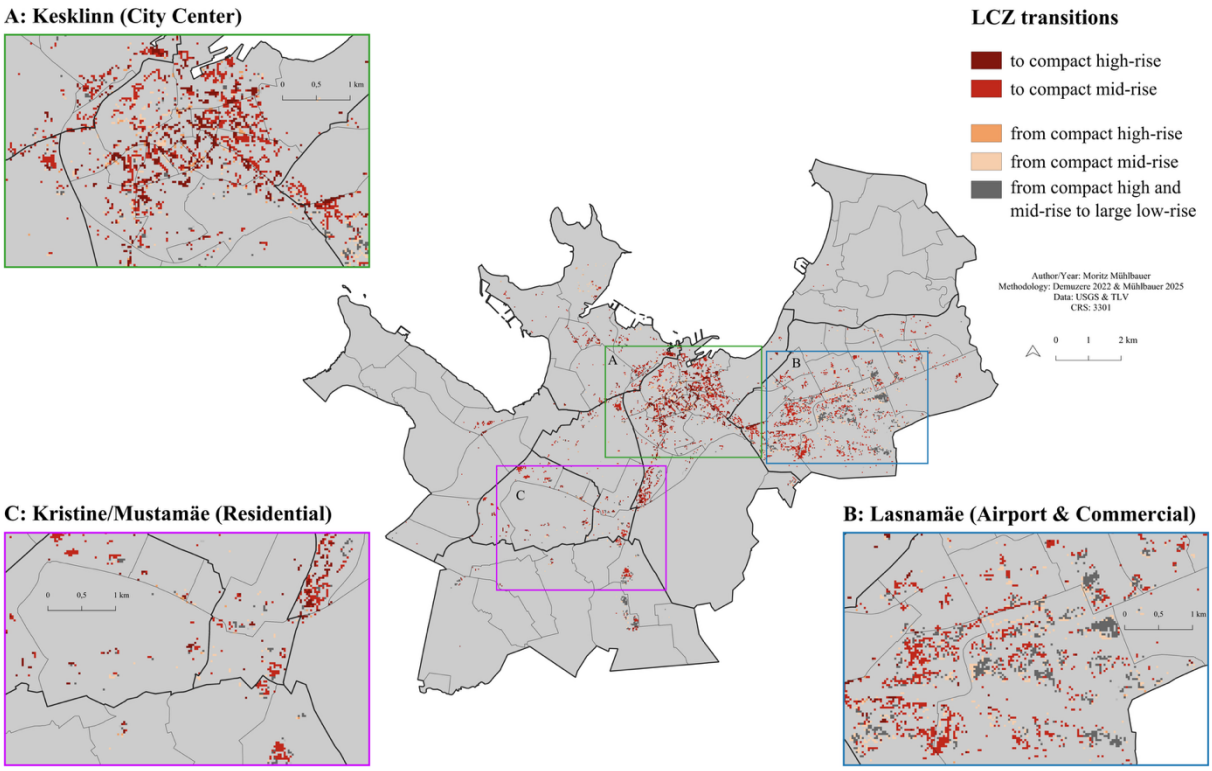

Figure 9: Intra-urban LCZ transitions from 2014 to 2022

4.2 Surface Urban Heat Islands in Tallinn – 2014 and 2022

4.2.1 Land surface temperature distribution within Local Climate Zones

Figure 10 depicts box plots representing the distribution of LST within LCZs. The boxes indicate the median and the first/third quartiles. The whiskers are extended to the minimum and maximum LST for each LCZ. Additionally, each date is assigned the standard deviation, the overall LST median, and the maximum air temperature measured that day.

Urban LCZs exhibit markedly higher LSTs compared to the natural zones A (dense trees) and B (scattered trees) throughout all dates, with LCZ 1 (compact high-rise), LCZ 2 (compact mid-rise), and LCZ 8 (large low-rise) showing the highest median values. Additionally, compact zones proved to be hotter than the open ones, LCZ 4 (open high-rise) and LCZ 5 (open mid-rise). In contrast, LCZ A and B demonstrate substantially and consistently lower LSTs, with medians around or below 30 °C.

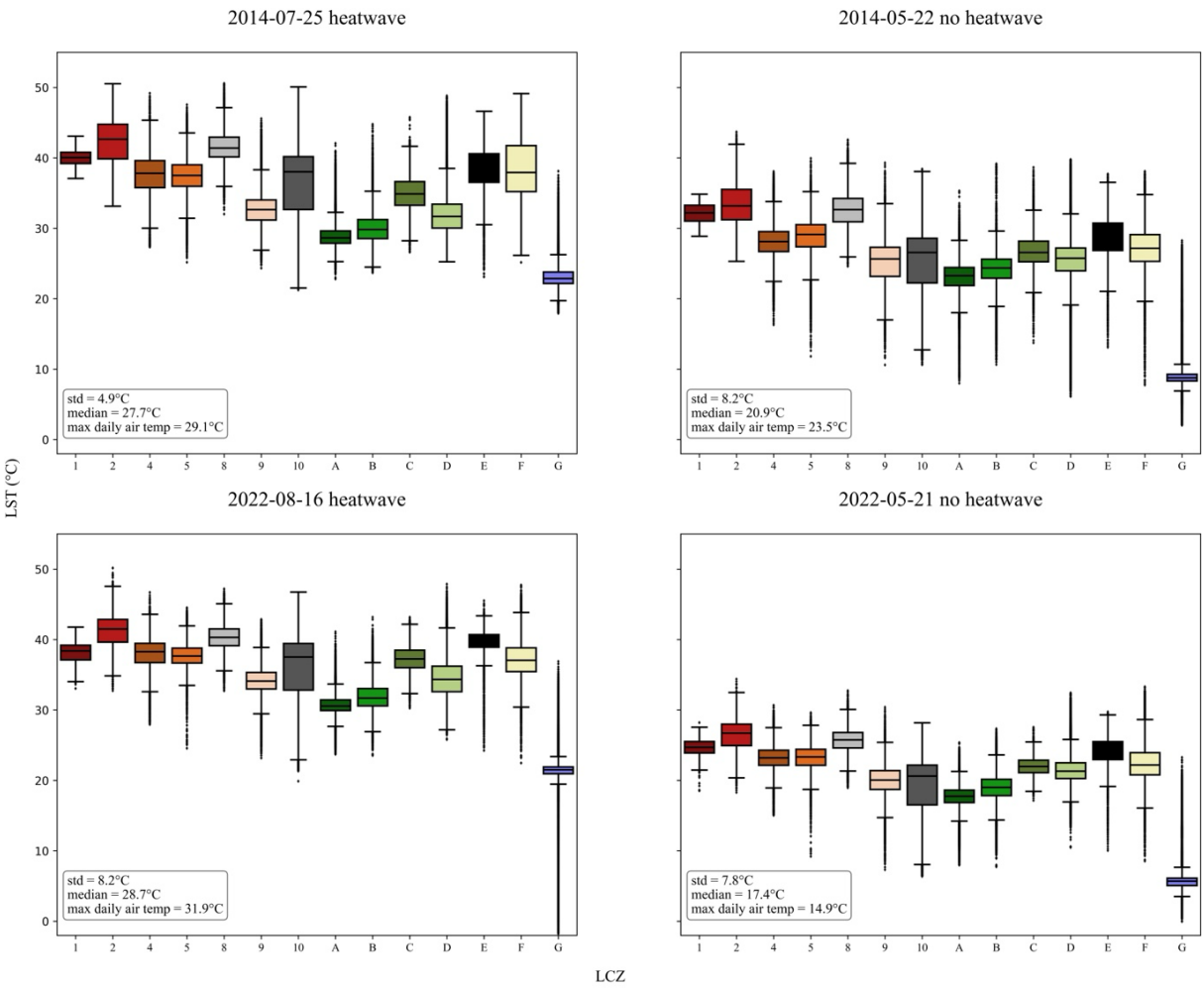

Figure 10: LST distribution within LCZs for heatwave and non-heatwave days in 2014 and 2022, LCZ key: 1 - Compact high-rise, 2 – Compact mid-rise, 4 – Open high-rise, 5 – Open mid-rise, 8 – Large low-rise, 9 – Sparsely built, 10 – Heavy Industry, A – Dense trees, B – Scattered trees, C – Bush and scrub, D – Low plants, E – Paved or bare rock, F – Bare soil or sand, G - Water

LCZ 9 (sparsely built) is the coolest built-up zone, always being lower than open and especially compact ones. LCZ 10 (industry) shows wider interquartile ranges and is significantly hotter than A and B.

LCZ C (Bush and scrub) and D (Low plants) are the hottest out of the vegetated zones, with LCZ D denoting wide interquartile ranges and a high LST variability. LCZ E (paved) and F (soil/sand) exhibit significantly higher temperature values than A-D, being equal to or hotter than openly built-up zones. Notably, the lowest LSTs are observed in LCZ G (water), reinforcing the cooling role of water bodies during extreme heat events.

When looking into the differences between heatwave and non-heatwave days, it becomes evident that heatwaves increase the LST of all LCZs in both years. In 2014, the heatwave median LST temperature increased by 6.8 °C and the maximum daily air temperature by 5.6 °C.

The 2014 heatwave especially increased the LST from LCZs, which this study considers urban. The median LST of LCZs 1, 2, and 8 surpassed the 40 °C mark, proving the heating of urbanized areas under extreme temperature conditions. Notably, LCZ E shows a significant LST surge just below 40 °C, indicating a similar response of artificial and impervious surfaces to extreme heat. The same can be stated for non-vegetated bare soil/sand areas of LCZ F, industry (LCZ 10), and for the built-up open zones 4 and 5. In contrast, LCZ 9 did not heat up as strongly as the other built types, highlighting the importance of vegetation between urbanized infrastructure. Adding to this, the LST of LCZs A, B, and D was not significantly elevated by the heatwave, with the median remaining around 30 °C. This stresses the importance of green buffer zones within cities to compensate for the hot urbanized areas under extreme heat exposure.

In 2022, the LST difference between heatwave and non-heatwave conditions is even more pronounced than in 2014. The heatwave median LST increased by 11.3 °C, and the maximum daily air temperature rose by 17 °C. As in 2014, urban LCZs showed a stronger amplification of LST under heatwave conditions compared to vegetated ones. LCZs 1–10, E, and F recorded the highest medians, around 40 °C, and the most substantial increases, except for sparsely built LCZ 9. LCZs A and B remained the coolest, with LSTs around 30 °C. Among vegetated zones, LCZs C and D experienced the most notable temperature surges. At nearly 39 °C, LCZ C is almost as hot as LCZs 4 and 5. LCZ D is significantly warmer than A and B, and comparable in LST to LCZ 9.

Comparing 2014 and 2022, Figure 10 shows that heatwaves had a similarly strong increasing effect on LST across LCZs, particularly in LCZs 1, 2, 8, and E. The cooling influence of water remains evident, with dense trees being the second coolest non-urban class. Between 2014 and 2022, the median LST of LCZs increased by 1 °C during heatwaves and decreased by 3.5 °C during non-heatwave periods.

Examining LST differences within LCZs on heatwave days between 2014 and 2022, LCZ 1 remained below 40 °C in 2022. LSTs in other built-up classes showed no significant change.

LCZs A and B increased slightly, exceeding 30 °C, while LCZs C and D rose to approximately 39 °C and 35 °C, respectively.

The non-heatwave day in 2022 had significantly lower air temperatures, resulting in a clearly reduced LST. LSTs across all LCZs were lower compared to 2014, yet the overall pattern remained consistent: urbanized and impervious zones were hotter than vegetated and pervious ones. This highlights the heating effect of dense urban morphology and paved surfaces, even under non-extreme conditions.

In summary, while temperature differences between LCZs persist under non-heatwave conditions, they are less pronounced than during heatwaves, emphasizing the amplifying effect of extreme heat on thermal contrasts within urban areas. Green buffer zones and water bodies remain effective in mitigating urban heat stress. These findings reinforce the strong thermal footprint of built-up LCZs under both typical and extreme conditions.

4.2.2 Impact of urban morphology and heatwaves on intensity

This section analyses the impact of urban morphology and heatwaves on SUHI intensity through SUHI maps matching the distribution of LCZs. **Figure 11** displays the spatial distribution and intensity of SUHI as an urban-rural difference for heatwave and non-heatwave days in 2014 and 2022. The intensity is calculated in relation to the mean LST of the reference zone D – low plants.

The maps reveal a pronounced SUHI core centered in and around Kesklinn and in Lasnamäe, Mustamäe, and Kriistine, where the intensity goes up to +8 °C. These hotspots are spatially aligned with densely built LCZs, particularly compact mid- and high-rise, as well as large low-rise and paved, confirming the strong thermal impact of high-density urban development. The extensive open mid and high-rise areas are more volatile in relation to their heating. These areas can heat up significantly, but always stay below the intensity of compact and large zones.

In contrast, sparsely built zones consistently show an intensity of 0 °C equal to the reference zone or less. This proves that less densely developed residential districts with vegetation are less susceptible to heating during extreme weather events. Dense and scattered trees steadily demonstrate negative SUHI intensity, making them cooling green buffers in between the heated urban structures. Water yields the lowest intensity out of all LCZs, staying below 6 °C constantly. The different water intensity on the 2014 heatwave day can be explained by cloud

artifacts contaminating the Landsat satellite image and being very cold (- 1°C), and therefore biasing the overall LST mean of water.

When looking into the differences between heatwave and non-heatwave days, it becomes evident that heatwaves increase the SUHI intensity in both years.

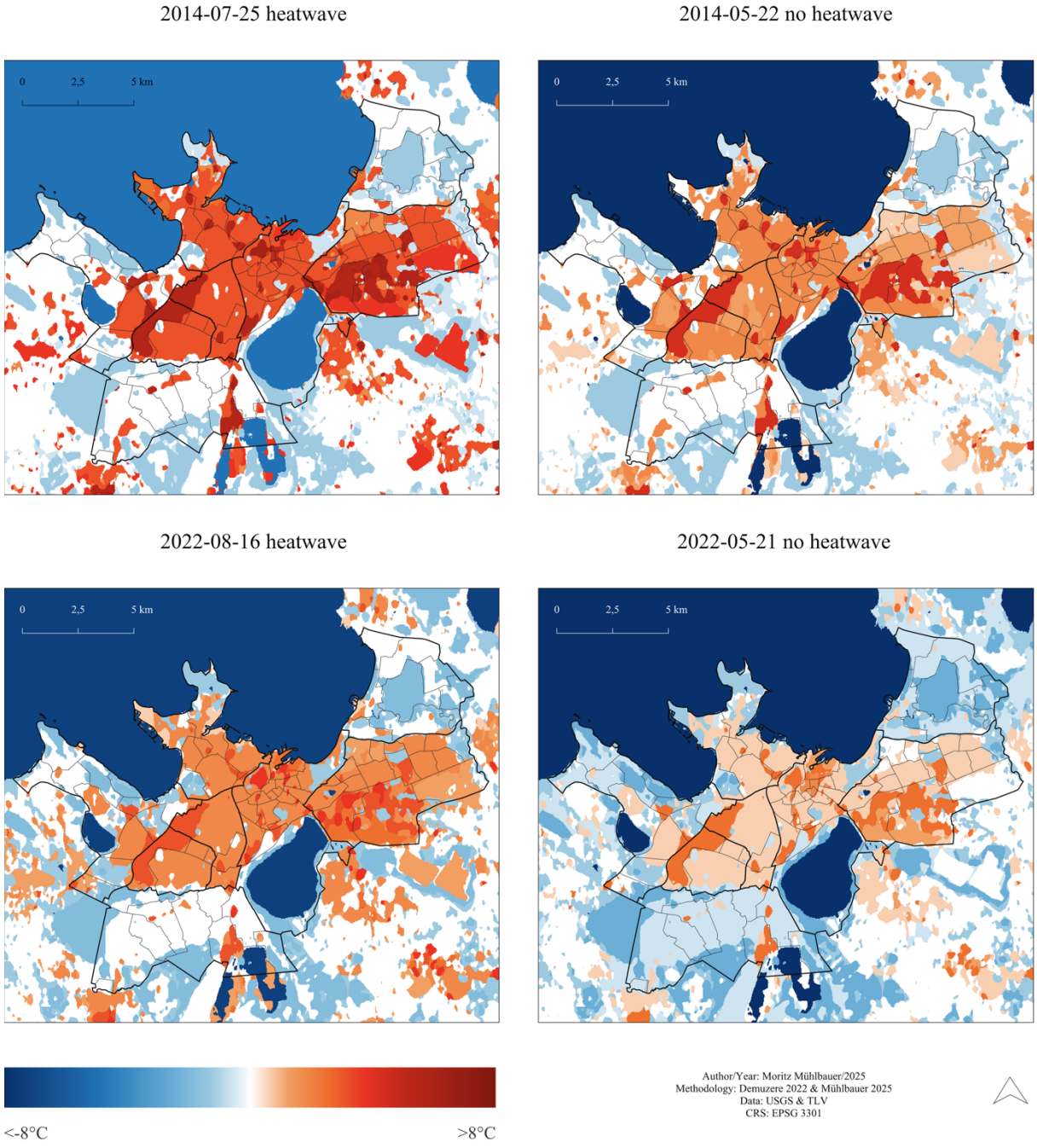

Figure 11: SUHI intensity on heatwave and non-heatwave days in 2014 and 2022

In 2014, the aggravating effect of heatwaves on SUHIs was especially strong. The compact mid or high-rise city center Kesklinn has an intensity of + 8 °C or more. The large low-rise zone of Lasnamäe surpasses +8 °C, and the neighboring paved airport shows an equally high value of

+6 °C. Open high-rise areas are as hot as the open mid-rise ones in Mustamäe/Kriistine (+5 °C), the bare soil/sand in the East heats up even more (+ 6 °C), and the bush/scrub zone lies at +2 °C.

In contrast, sparsely built areas of Nõmme, Haabersti, and Pirita are significantly cooler, being assigned an intensity of 0 °C and thus equal to the reference zone. Dense and scattered trees, water bodies, and some parts of the low-density residential zones exhibit negative SUHI intensity values (≤ -2 °C), suggesting cooler-than-reference conditions. Notably, water bodies such as Lake Ülemiste and Tallinn Bay exhibit strong negative SUHII values (up to -8 °C), further reinforcing their moderating effect during heat extremes.

The non-heatwave day in 2014 shows similar spatial patterns but a decreased intensity. The compact mid and high-rise zones in Kesklinn and Lasnamäe, and the large low-rise zones in Mustamäe, Kriistine, and Lasnamäe remain the most intense (8 °C or more). The open mid-rise zone spanning all the previously mentioned districts is the second hottest zone, together with the paved zone of Tallinn airport (+ 3 °C). Open high-rise areas in Kristiine, Lasnamäe, and Mustamäe are slightly cooler (+ 2 °C).

Sparsely built areas at the borders of the municipality did not heat up compared to the reference zone (0 °C). Heavy industry at the northern tip in Põhja-Tallinna cooled down significantly from + 4 °C during the heatwave to 0 °C on the non-heatwave day. Vegetated zones and water keep their negative intensity between -2 and -8 °C.

In 2022, heatwaves likewise increased the SUHI intensity and especially heated up compact and large low-rise zones (+ 6 °C). Open mid-rise remains between the two extremes, showing an intensity of 4 °C. Sparsely built, vegetated, and water zones maintain their intensities <= 0 °C.

The non-heatwave SUHI intensity of 2022 is the overall lowest measured in this analysis. Compact mid-rise and large low-rise remain the hottest zones with an intensity of +4 °C. Compared to the heatwave day, the temperature dropped around 2 °C in those zones. Paved and compact high-rise areas deviate from the reference zone by +2 °C, making them hotter than open mid-rise (+1 °C). The sparsely built zone moves down to negative intensity among the dense and

scattered trees (- 2 to - 6 °C) and water (< - 8 °C). Bush/scrub and bare soil/sand are as hot as the reference zone, hence having an intensity of 0 °C.

When comparing the years, it becomes evident that the intensities measured in 2014 are higher than 2022. During heatwaves, it can be observed that the intensity across all zones is lower than in 2022, and no zone exceeds the + 8 °C intensity threshold. The most remarkable change is the reduced intensity of the compact high-rise zone in Kesklinn, now only being 4 °C hotter than the reference zone, integrating into the open mid-rise area. Furthermore, paved, heavy industry, and open high-rise zones show diminished intensities between + 1 and 2 °C.

Summing up, the SUHI intensity hotspots remained spatially stable over compact areas in Kesklinn and large low-rise surfaces in Lasnamäe, Mustamäe, and Kriistine, but heatwaves increased their intensity in both years. Sparse residential areas at the eastern and western borders of Tallinn, regardless of the weather condition, do not heat up more than the reference zone, and vegetated zones and water have a cooling effect.

4.2.3 Impact of urbanization on magnitude

This chapter analyses the spatially visualized SUHI, previously presented through maps, by the area of SUHIs (pixels assigned an intensity > 0 °C), allowing conclusions about the impact of urbanization from 2014 to 2022. This provides insights into the magnitude of SUHIs and a more differentiated understanding of their intensity during heatwave and non-heatwave days.

Figure 12 depicts the area of SUHIs classified by their intensity per year and heatwave/non-heatwave day along the mean temperature of the reference zone D and the overall mean LCZ temperature. Water has been excluded from the overall mean due to its cloud bias.

On the non-heatwave day in 2014, the total SUHI area measured 70.38 km². The most common intensity class was 2 (35.2 km²), followed by class 1 (21.05 km²) and class 4 (13.79 km²), while class 3 covered only a small area (0.34 km²), and no intensities above 8 °C were observed. In contrast, the heatwave day that year showed a slightly larger SUHI area of 72 km². Class 3 dominated (52.33 km²), followed by class 5 (13.79 km²) and class 2 (5.54 km²). Class 4 remained minimal (0.34 km²), and class 1 was absent.

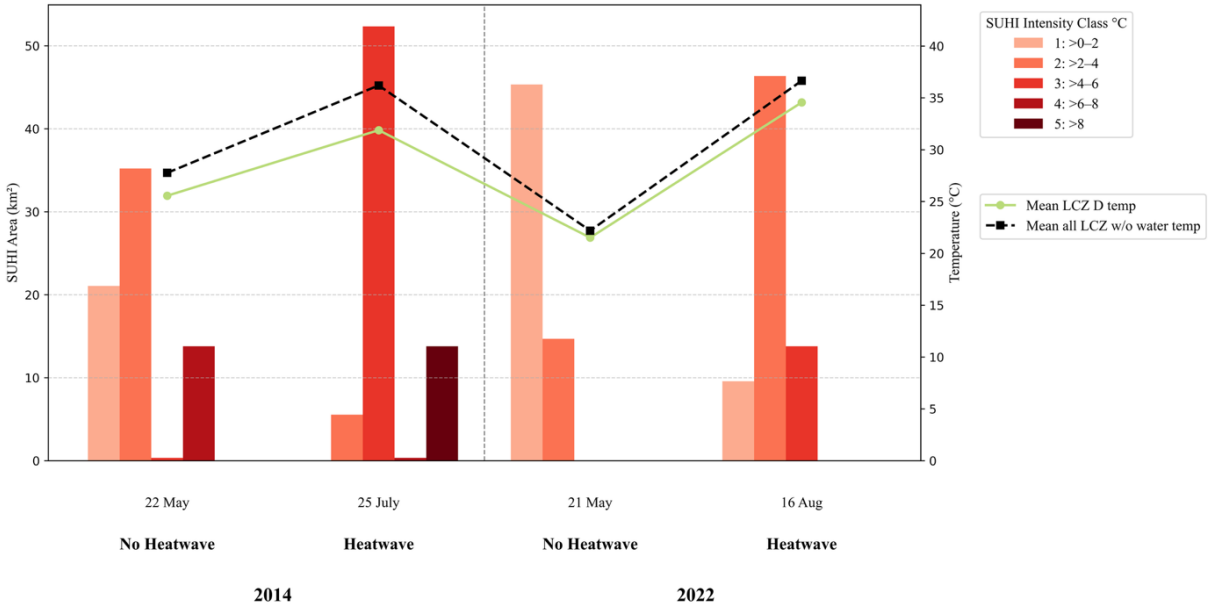

Figure 12: SUHI area by intensity class for heatwave and non-heatwave days in 2014 and 2022

In 2022, the non-heatwave day had the lowest total SUHI area, at 60.03 km². Class 1 was the most widespread (45.34 km²), followed by class 2 (14.69 km²), with no higher intensity classes recorded, indicating generally low SUHI intensity. On the heatwave day in 2022, the SUHI area increased to 69.71 km². Class 2 was the most extensive (46.35 km²), followed by class 1 (9.58 km²) and class 3 (3.78 km²); other classes were not present.

Overall, the analysis confirms that SUHI magnitude is consistently greater during heatwaves compared to non-heatwave days in both years. However, there is a clear decline in total SUHI coverage from 2014 to 2022: a reduction of 10.35 km² on non-heatwave days and 2.29 km² on heatwave days. Therefore, despite findings from section 4.1.3, no clear intensifying effect of urban densification on SUHI extent could be confirmed.

5 Discussion

5.1 Reflection on data and methods

The from-scratch and self-developed methodology for multi-temporal LCZ mapping was able to accurately select training areas and produce LCZ maps reflecting the real urban environment in Tallinn for 2014 and 2022.

The matter of scale has been the most challenging part in this regard. This study produced LCZ maps with a resolution of 30 m, trying to capture zones as precisely as possible while still operating on a local scale and avoiding resampling of Landsat LST satellite imagery. While the

resolution choice achieved great and detailed results on the building height, the density indicator, built fraction, resulted in rather noisy outputs for sparse, large, and open zones. Additionally, large buildings covering multiple cells caused high density values, indicating an urban center, while they were only peripheral warehouses. In retrospect, a moving window operation over both building and land cover data could have facilitated the TA selection process by registering a broader spectrum of conditions.

Nevertheless, the overall trend of increasing densification from the remote districts towards Kesklinn could be captured. For future research, it would be interesting to test the same analysis with a resolution of 100 m to explore the trade-off between richness of detail and generalization.

The connection of LCZs with LST via thermal LCZs revealed solid insights into the urban climate of Tallinn and the heating of urbanized parts compared to rural ones, as well as the accelerating effect of heatwaves. However, the limited satellite availability hindered a month-to-month and even more so day-to-day comparison between 2014 and 2022. Beyond this, temperature and climate-related studies need to be conducted over a long period of time to achieve the most representative results. The chosen sample dates allow, nonetheless, sound and directive conclusions about the effect of urbanization and heatwaves on SUHI intensity.

Lastly, the quality of the vector datasets was rather mediocre, referring to the bulk of missing data and the necessary height estimation and gap-filling procedure. In addition, this study was limited to the years 2014 and 2022 due to the availability of the vector datasets. Presumably, a more significant urban sprawl and densification could have been detected when going back further in time.

5.2 Limitations of the Local Climate Zone concept

The LCZ concept proved to be a useful framework to generalize urban research and make heterogeneous study areas around the world comparable. Nevertheless, the universal concept of LCZs generalizes intentionally, which may lead to oversimplified results when applying the same schema to a broad variety of urban extents all around the world. Therefore, this study sought to tailor the concept to the study area of Tallinn to the maximum by incorporating the external building and land cover datasets.

Moving on to complications caused by the reference zone D (low plants), which functions as the threshold for assessing the temperature difference between urban and rural areas. This zone is considered to be the best pick for a balanced measure of the SUHI intensity because it appears

within the borders of cities as well as in the outer peripheral areas and usually shows a lower temperature profile than built-up and urban zones.

In the case of Tallinn, LCZ D appeared to be a rather bad choice. First, due to its volatile temperature profile across heat and non-heatwave days, and second, because of its high temperature in general and specifically during heatwave days, biasing the SUHI effect. In discussion with Dr. Valentina Sagris, it became apparent that the varying temperatures are mainly caused by the zone being agricultural land, which is subject to seasonal fluctuations caused by mowing and harvesting of fields. In addition, natural grasslands of northern Estonia have a clay-like soil with thin layers of fertile humus and sparse vegetation cover, which heat up very strongly, especially during heatwaves.

Concluding, the author advocates for deviating from the standard approach and choosing the reference zone A (dense trees) when analyzing SUHI intensity in Tallinn. It has proven to be a constantly cool zone and is sufficiently present within the Tallinn municipality. Also, the LCZ B scattered trees, which are represented in Tallinn by the large park of Kadriorg, can be a candidate for this threshold in urban space due to its cooling effect. This gain in knowledge can be considered for future research.

Lastly, the classification thresholds for LCZs are not perfectly applicable to the Estonian case. Referring to Dr. Valentina Sagris again, residential districts of Nõmme, Haabersti, and Pirita do not sound as ‘sparsely built-up’ for the Estonian ear. They would be considered open low-rise with respect to the sparse settlement of Estonia overall. This can be attributed to the generalising concept, as described above.

5.3 Interpretation and contextualization of the results

The LCZ maps built the basis for the analysis of urban sprawl and densification, and of the dynamics of SUHI intensity. The overall accuracy of both maps surpassed the minimum accuracy threshold. The classification accuracy of certain zones varies significantly due to different sample sizes or intra-zone heterogeneity across the study area. The presence of outliers, particularly in industrial and vegetated zones, may be attributed to localized microclimatic effects or spatial heterogeneity within the LCZ polygons. The high variability of LST of water is due to

cloud artefacts over Tallinn Bay, biasing the overall mean with their extremely low temperature of ~-1 °C.

The wider interquartile ranges across most LCZs, especially industrial (LCZ 10) and sparsely built (LCZ 9), suggest internal heterogeneity and potential variation in material properties, shading, or surface moisture, which may reflect climatic differences on the selected dates or changes in surface materials.

Continuing with the insights derived from the LCZ mapping, this study could not find an indicator for urban sprawl within the Tallinn municipality by comparing the total area of urban LCZs from 2014 and 2022. However, this growth is happening outside its borders (Sagris & Sepp, 2017).

First, due to limited space within the municipality's borders, real estate development is naturally constrained. According to Dr. Valentina Sagris, the bulk of the urban land grabbing is taking place outside or right at the borders of the municipality, reflecting a typical process of city expansion. This corresponds to the established densification of Kesklinn. The district and others at lower speeds tend to densify instead of the urban area expanding overall.

Second, for each year, only the corresponding training area set representative of that specific year was used in generating the LCZ map. Consequently, differences in LCZ classifications between years may occur even in areas where no actual land cover changes took place, due to imagery signal variations in the year-specific training area sets (Demuzere, 2022). The author concludes that the observed slight decrease in urban LCZ area is a result of the limited training areas used, rather than reflecting an actual change.

Moving on to the dynamics of SUHI intensity, the results prove an enhancement of the effect of heatwaves. Besides, a general decrease in SUHI extent (area) and intensity (magnitude by class from 1-5) comparing 2014 and 2022 was found, even though SUHI hotspots like Kesklinn and Lasnamäe have been densified.

The SUHI intensity is calculated in relation to the reference zone, making its temperature a decisive factor. The previously explained complications of reference zone D partially explain the lower intensities of 2022. The mean temperature of LCZ D in 2014 (31.8 °C) and 2022 (34.6 °C) differs by 2.8 °C, while the overall mean LST of LCZs remained at around 36 °C, decreasing the overall intensity by more than one class range. For the 2022 non-heatwave case, the

reference zone's temperature almost equals the overall mean, making it again not an ideal representation of cooler areas, unlike LCZ A.

Aside from the biasing SUHI reference, the selection of single images plays an important part in unexpected intensity patterns as well. Temporal tiles extracted from one day can be influenced by various factors not respected, especially for coastal cities. Future studies could achieve more accurate results by considering windspeed and direction, humidity, precipitation, and solar radiation. Additionally, the selected heatwave images are not representative of their period nor all heatwave occurrences that year. Also, images were taken on different dates – July 2014 and August 2022, therefore, the difference in LST can be due to the seasonal stage of low vegetation and farming activities.

6 Conclusion

This study investigated urbanization through the lenses of urban sprawl and densification, as well as the intensity and magnitude of SUHIs during heatwave and non-heatwave days in the Tallinn municipality, comparing the years 2014 and 2022. The primary aim was to quantify urbanization over this period and assess the amplifying effect of both urbanization and heatwaves on SUHI intensity.

LCZ maps were generated for both years to serve as the foundation for analysing urban change and SUHI patterns. A key contribution of this work was the author's adaptation of the official multi-temporal LCZ mapping scripts, which preserved their functionality following the migration of Landsat data from Collection 1 to Collection 2. These adjustments were integrated into the default processing workflow of Demuzere (2022).

Training area selection for the LCZ classification was facilitated by building and land cover datasets, as well as Landsat 8 imagery, ensuring a scientifically robust basis for supervised classification. LST data was used to derive thermal statistics of LCZs and evaluate the influence of heatwaves on SUHI intensity.

In response to research question 1, which asked which districts in Tallinn experienced changes in the built environment, such as densification or urban sprawl, between 2014 and 2022, the results indicate a clear pattern of densification, particularly in and around Kesklinn, with no significant signs of urban sprawl within the municipality's administrative boundaries. The net increase in compact urban LCZs through internal transitions was +2.44 km², while the total area

of urban LCZs decreased by 2 km². This suggests that urban growth may be extending beyond the administrative limits of Tallinn.

Addressing research question 2, which explored how urban morphology influences the intensity of SUHIs in Tallinn, the spatial distribution of SUHI intensity shows that compact, impervious zones, characterized by dense building coverage and sealed surfaces, experienced the highest levels of excess heat. In contrast, areas that are vegetated, sparsely built, or feature rainwater-pervious surfaces acted as effective thermal buffers. These findings underscore the strong correlation between dense, sealed urban morphology and elevated SUHI intensity, and highlight the critical role of strategic land use planning and green infrastructure in mitigating urban heat impacts.

With regard to research question 3, which examined the extent to which urbanization in Tallinn, between 2014 and 2022, has influenced the intensity and magnitude of SUHIs, the findings suggest that, despite localized densification, particularly in central districts, there was no clear overall increase in SUHI intensity or spatial extent over the study period. This indicates that urbanization during this time did not produce a consistent or direct enhancing effect on SUHI development across the city. While some areas experienced morphological change, the broader urban fabric did not exhibit a uniform intensification of heat island effects attributable to urban growth alone.

In addressing research question 4, which explored the effect of heatwaves on SUHI intensity in Tallinn, the analysis reveals that SUHI intensity was consistently higher during heatwave periods, compared to non-heatwave days. For example, during a heatwave in 2014, the extent of the SUHI increased by 1.63 km², while in 2022, it expanded significantly by 9.68 km². These findings confirm the amplifying impact of extreme heat events on SUHI formation, especially in compact, paved, and large low-rise zones. This highlights the vulnerability of dense urban areas to thermal stress during extreme weather and reinforces the importance of integrating cooling features, such as vegetation and water bodies, into urban planning strategies to mitigate heat accumulation.

Future research could refine the reference zone selection, e.g., using LCZ A or B, to better align with soil and land cover conditions specific to northern Estonia, avoiding the seasonal bias introduced by harvested farmland and alvar grasslands. Expanding the analysis to include years prior to 2014 may better capture long-term urbanization trends and provide deeper insights into how extended and densified morphology has shaped Tallinn's urban climate over recent

decades. Additionally, incorporating more satellite imagery from the onset, peak, and recovery phases of heatwaves could improve our understanding of the temporal dynamics and lasting impact of extreme weather on urban climate in Tallinn.

7 Summary

Kokkuvõte

Pinnalähedaste soojussaarte dünaamika linnas ja kuumalainete mõju kohalike kliimatsoonide kaardistamise kaudu Tallinnas aastatel 2014 ja 2022.

Moritz Mühlbauer

Käesolevas uurimistöös analüüsitakse linnastumist ja linnade pinnalähedase soojussaare intensiivsust (*Surface Urban Heat Island Intensity, SUHII*) Tallinnas aastatel 2014 ja 2022, keskendudes kuumalaine ja tavatingimuste võrdlemisele. Eesmärgiks oli kvantifitseerida linnastumist valitud ajavahemikul ning hinnata linnastumise ja kuumalainete süvendavat mõju SUHII-le.

Linnastumise ja SUHII analüüsi alusena koostati mõlema aasta kohta kohalike kliimatsoonide (*Local Climate Zone, LCZ*) kaardid. Klassifikaatori õpetamispiirkondade (*training areas, TA*) valimist LCZ kaardistamiseks toetasid hoonete ja maakatte andmekogumid ning Landsat 8 pildimaterjal; TAd oli sisendiks näidistega klassifitseerimise (*supervised classification*) jaoks. LST (*Land Surface Temperature*) kaarte kasutati LCZ-de termiliste omaduste tuletamiseks ja kuumalainete mõju hindamiseks SUHII-le.

Tulemused näitasid asustuse tihenemist Kesklinnas ja selle ümbruses, kuid Tallinna linna administratiivpiirides valglinnastumist ei tuvastatud. SUHII ruumiline jaotus kinnitas, et kõige rohkem liigset soojust esines tihedalt hoonestatud kõvakattega aladel, samas kui taimestikuga kaetud, hõredalt hoonestatud ja vett läbilaskvad alad toimisid soojuspuhvritena. See rõhutab maakasutuse planeerimise ja rohelise infrastruktuuri tähtsust linnade soojusstressi leevendamisel kliimamuutuse tingimustes.

SUHII oli kuumalainete ajal oluliselt suurem, mis toob välja taimestiku ja veekogude jahutusfunktsioonide suurenevat tähtsust, eriti kompaktsetes, sillutatud ja madala suurhoonestuse aladel.

Aastatel 2014 – 2022 ei täheldatud SUHII ulatuse või intensiivsuse üldist suurenemist, vaatamata asustuse kohalikule tihenemisele. Tulevastes uuringutes võiks täpsustada referentskliimatsooni valikut SUHII lävendi leidmiseks, laiendada ajalist vahemikku ning kasutada paremad hoonete ja maakatte andmeid, suurendades seeläbi LCZ kaardistamise ja SUHII hindamise täpsust Tallinnas.

8 References

Alexander, C. (2020). Normalised difference spectral indices and urban land cover as indicators of land surface temperature (LST). *International Journal of Applied Earth Observation and Geoinformation*, *86*. https://doi.org/10.1016/J.JAG.2019.102013

Alghamdi, A. S., Alzhrani, A. I., & Alanazi, H. H. (2021). Local climate zones and thermal characteristics in Riyadh City, Saudi Arabia. *Remote Sensing*, *13*(22). https://doi.org/10.3390/RS13224526

Aslam, A., & Rana, I. A. (2022). The use of local climate zones in the urban environment: A systematic review of data sources, methods, and themes. *Urban Climate*, *42*, 101120. https://doi.org/10.1016/J.UCLIM.2022.101120

Bechtel, B., Alexander, P. J., Böhner, J., Ching, J., Conrad, O., Feddema, J., Mills, G., See, L., & Stewart, I. (2015). Mapping Local Climate Zones for a Worldwide Database of the Form and Function of Cities. *ISPRS Int. J. Geo-Inf*, *4*, 199–219. https://doi.org/10.3390/ijgi4010199

Brozovsky, J., Gaitani, N., & Gustavsen, A. (2021). A systematic review of urban climate research in cold and polar climate regions. *Renewable and Sustainable Energy Reviews*, *138*, 110551. https://doi.org/10.1016/J.RSER.2020.110551

Debbage, N., & Shepherd, J. M. (2015). The urban heat island effect and city contiguity. *Computers, Environment and Urban Systems*, *54*, 181–194. https://doi.org/10.1016/J.COMPENVURBSYS.2015.08.002

Demuzere, M. (2022). *multitemporal-lcz-mapping*. Retrieved 26 May 2025, from https://github.com/matthiasdemuzere/multitemporal-lcz-mapping

Demuzere, M., Kittner, J., & Bechtel, B. (2021). LCZ Generator: A Web Application to Create Local Climate Zone Maps. *FRONTIERS IN ENVIRONMENTAL SCIENCE*, *9*. https://doi.org/10.3389/fenvs.2021.637455

Demuzere, M., Mihara, T., Redivo, C. P., Feddema, J., & Setton, E. (2020). *Multi-temporal LCZ maps for Canadian functional urban areas*. https://doi.org/10.31219/OSF.IO/H5TM6

EEA. (n.d.). *Estonian weather agency, Meterological services*. Retrieved 26 May 2025, from https://www.lennuilm.ee/?lang=en

Emmanuel, R., & Loconsole, A. (2015). Green infrastructure as an adaptation approach to tackling urban overheating in the Glasgow Clyde Valley Region, UK. *Landscape and Urban Planning*, *138*, 71–86. https://doi.org/10.1016/J.LANDURBPLAN.2015.02.012

Frich, P., Alexander, L. V., Della-Marta, P., Gleason, B., Haylock, M., Tank Klein, A. M. G., & Peterson, T. (2002). Observed coherent changes in climatic extremes during the second half of the twentieth century. *Climate Research*, *19*(3), 193–212. https://doi.org/10.3354/CR019193

Geletič, J., Lehnert, M., Savić, S., & Milošević, D. (2018). Modelled spatiotemporal variability of outdoor thermal comfort in local climate zones of the city of Brno, Czech Republic. *Science of The Total Environment*, *624*, 385–395. https://doi.org/10.1016/J.SCITOTENV.2017.12.076

Jaagus, J., Rimkus, E., Briede, A., Sagris, V., Aasa, A., Kapilovaite, J., & Sepp, M. (2024). Long-term changes in heat wave parameters in the eastern Baltic region. *Theoretical and Applied Climatology*, 1–16. https://doi.org/10.1007/S00704-024-04925-7/FIGURES/10

Khoshnoodmotlagh, S., Daneshi, A., Gharari, S., Verrelst, J., Mirzaei, M., & Omrani, H. (2021). Urban morphology detection and it's linking with land surface temperature: A case study for Tehran Metropolis, Iran. *Sustainable Cities and Society*, *74*, 103228. https://doi.org/10.1016/J.SCS.2021.103228

Liu, L., Lin, Y., Xiao, Y., Xue, P., Shi, L., Chen, X., & Liu, J. (2018). Quantitative effects of urban spatial characteristics on outdoor thermal comfort based on the LCZ scheme. *Building and Environment*, *143*, 443–460. https://doi.org/10.1016/J.BUILDENV.2018.07.019

Perkins, S. E. (2015). A review on the scientific understanding of heatwaves—Their measurement, driving mechanisms, and changes at the global scale. *Atmospheric Research*, *164–165*, 242–267. https://doi.org/10.1016/J.ATMOSRES.2015.05.014

Perkins, S. E., & Alexander, L. V. (2013). On the Measurement of Heat Waves. *Journal of Climate*, *26*(13), 4500–4517. https://doi.org/10.1175/JCLI-D-12-00383.1

Sagris, V., & Sepp, M. (2017). Landsat-8 TIRS Data for Assessing Urban Heat Island Effect and Its Impact on Human Health. *IEEE GEOSCIENCE AND REMOTE SENSING LETTERS*, *14*(12). https://doi.org/10.1109/LGRS.2017.2765703

Stewart, I. D., & Oke, T. R. (2012). Local Climate Zones for Urban Temperature Studies. *Bulletin of the American Meteorological Society*, *93*(12), 1879–1900. https://doi.org/10.1175/BAMS-D-11-00019.1

TLV. (n.d.). *Tallinn Geoportal*. Retrieved 26 May 2025, from https://www.tallinn.ee/et/geoportaal/ruumi-andmed

United Nations. (2024). *Global Issue: Population*. Retrieved 26 May 2025, from https://www.un.org/en/global-issues/population

USGS. (n.d.). *Landsat Normalized Difference Vegetation Index | U.S. Geological Survey*. Retrieved 26 May 2025, from https://www.usgs.gov/landsat-missions/landsat-normalized-difference-vegetation-index

USGS. (2018). *NDVI, the Foundation for Remote Sensing Phenology*. https://www.usgs.gov/special-topics/remote-sensing-phenology/science/ndvi-foundation-remote-sensing-phenology?utm_source=chatgpt.com

USGS. (2024). *Landsat Collection 1 to Collection 2 migration*. Retrieved 26 May 2025, from https://developers.google.com/earth-engine/landsat_c1_to_c2

Vaidya, M., Keskar, R., & Kotharkar, R. (2024). Quantifying the effect of surrounding spatial heterogeneity on land surface temperature based on local climate zones using mutual information. *Sustainable Cities and Society*, *107*, 105455. https://doi.org/10.1016/J.SCS.2024.105455

Žgela, M., Herceg-Bulić, I., Lozuk, J., & Jureša, P. (2024). Linking land surface temperature and local climate zones in nine Croatian cities. *Urban Climate*, *54*. https://doi.org/10.1016/J.UCLIM.2024.101842

Zha, Y., Gao, J., & Ni, S. (2003). Use of normalized difference built-up index in automatically mapping urban areas from TM imagery. *International Journal of Remote Sensing*, *24*(3), 583–594. https://doi.org/10.1080/01431160304987

Code documentation: https://github.com/moritzm99/Master-Thesis-2025-Moritz-M-hlbauer-Code-Documentation/tree/main

9 Annexes

Annex 1. LCZ property thresholds

Local climate zone (LCZ)	Sky view factor[a]	Aspect ratio[b]	Building surface fraction[c]	Impervious surface fraction[d]	Pervious surface fraction[e]	Height of roughness elements[f]	Terrain roughness class[g]
LCZ 1	0.2–0.4	> 2	40–60	40–60	< 10	> 25	8
Compact high-rise							
LCZ 2	0.3–0.6	0.75–2	40–70	30–50	< 20	10–25	6–7
Compact midrise							
LCZ 3	0.2–0.6	0.75–1.5	40–70	20–50	< 30	3–10	6
Compact low-rise							
LCZ 4	0.5–0.7	0.75–1.25	20–40	30–40	30–40	>25	7–8
Open high-rise							
LCZ 5	0.5–0.8	0.3–0.75	20–40	30–50	20–40	10–25	5–6
Open midrise							
LCZ 6	0.6–0.9	0.3–0.75	20–40	20–50	30–60	3–10	5–6
Open low-rise							
LCZ 7	0.2–0.5	1–2	60–90	< 20	<30	2–4	4–5
Lightweight low-rise							
LCZ 8	>0.7	0.1–0.3	30–50	40–50	<20	3–10	5
Large low-rise							
LCZ 9	> 0.8	0.1–0.25	10–20	< 20	60–80	3–10	5–6
Sparsely built							
LCZ 10	0.6–0.9	0.2–0.5	20–30	20–40	40–50	5–15	5–6
Heavy industry							
LCZ A	<0.4	>1	<10	<10	>90	3–30	8
Dense trees							
LCZ B	0.5–0.8	0.25–0.75	<10	<10	>90	3–15	5–6
Scattered trees							
LCZ C	0.7–0.9	0.25–1.0	<10	<10	>90	<2	4–5
Bush, scrub							
LCZ D	>0.9	<0.1	<10	<10	>90	<1	3–4
Low plants							
LCZ E	>0.9	<0.1	<10	>90	<10	<0.25	1–2
Bare rock or paved							
LCZ F	>0.9	<0.1	<10	<10	>90	< 0.25	1–2
Bare soil or sand							
LCZ G	>0.9	<0.1	<10	<10	>90	–	1
Water							

[a] Ratio of the amount of sky hemisphere visible from ground level to that of an unobstructed hemisphere

[b] Mean height-to-width ratio of street canyons (LCZs 1–7), building spacing (LCZs 8–10), and tree spacing (LCZs A–G)

[c] Ratio of building plan area to total plan area (%)

[d] Ratio of impervious plan area (paved, rock) to total plan area (%)

[e] Ratio of pervious plan area (bare soil, vegetation, water) to total plan area (%)

[f] Geometric average of building heights (LCZs 1–10) and tree/plant heights (LCZs A–F) (m)

[g] Davenport et al.'s (2000) classification of effective terrain roughness (z_0) for city and country landscapes. See Table 5 for class descriptions

Annex 2. Decryption, translation, and aggregation of vector data

Landcover TYYP-ID	Estonian	English	Raster Code
11	Inimtekkeline taimkattega	Artificial surface with vegetation	1
12	Inimtekkeline taimkatteta	Artificial surface without vegetation	2
13	Looduslik taimkattega	Natural surface with vegetation	3
14	Looduslik taimkatteta	Natural surface without vegetation	4
15	Ehitise alune maa	The underground building	2
21	Mere osa	Sea	5*
22	Seisuveekogu	Standing water reservoir	5
23	Vooluveekogu	Stream water body	5
100	Määramata tee	Unspecified road/path	6**
110	Kiirtee	Highway	6
120	Põhitänav	Main Street	6
130	Jaotustänav	Distribution street	6
210	Kõrvaltänav	Side street	6
220	Veotänav	Transport Street	6
230	Kvartalisisene tee	Road within the quarter	6
240	Jalgtänav	Pedestrian street	6
250	Jalgtee	Footpath	6
310	Sõidetav plats	Drivable square	6
320	Teepeenar	Roadbed	6
330	Muu plats	Other square	6
410	Kergliiklustee	Light traffic road	6
420	Jalgrattatee	Bicycle path	6

Building TYYP-ID	Estonian	English	Raster Code
1	Elukoondlik hoone	Residential	1
2	Ühiskondlik hoone	Public	2
3	Kõrvalhoone	Outbuilding (auxiliary)	3
4	Tootmishoone	Production building	4
5	Maa-alune garaaž	Underground garage	5
6	Maa-alune kelder	Underground cellar	5
7	Muu maa-alune hoone	Other underground building/construction	5
8	Muu hoone	Other building	6
0	Määramata	Unspecified	7

Annex 3. Satellite availabilities and heatwave occurrences

Heatwave period	Air temperature (°C)	Satellite image availability	Cloud free	Tallinn coverage
2014-05-23	29.5			
2014-05-24	30.3	No	-	-
2014-05-25	29.7			
2014-07-23	28.0			
2014-07-24	27.3			
2014-07-25	29.1	Yes	Yes	Yes
2014-07-26	29.2			
2014-07-27	31.2			
2014-07-28	32.0			
2014-07-29	27.9			
2014-07-30	29.5			
2014-07-31	29.8			
2014-08-03	30.0	Yes	Yes	Yes
2014-08-04	31.6			
2014-08-05	31.2			
2014-08-06	31.2			
2014-08-07	29.9			
2018-07-15	28.7			
2018-07-16	28.8	No	-	-
2018-07-17	29.3			
2018-07-18	27.2			
2018-07-24	27.1			
2018-07-25	29.2			
2018-07-26	28.4			
2018-07-27	28.0	Yes	Yes	Yes
2018-07-28	28.5			
2018-07-29	34.2	Yes	No	Yes
2018-07-30	32.5			
2018-07-31	31.3			
2018-08-01	31.0			
2018-08-02	29.8			
2018-08-03	27.3			
2019-06-04	27.4			
2019-06-05	27.5	2x Yes	No/No	Yes/Yes
2019-06-06	31.1			
2019-06-07	30.0			
2019-06-08	29.6			
2020-06-26	27.7			
2020-06-27	28.9	No	-	-
2020-06-28	27.7			

2021-06-18	28.6			
2021-06-19	30.3	Yes	Yes	Yes
2021-06-20	31.8			
2021-06-21	32.5			
2021-06-22	32.6			
2021-06-23	30.2			
2021-07-05	29.0	Yes	No	Yes
2021-07-06	29.6			
2021-07-07	30.2			
2021-07-13	27.3			
2021-07-14	28.7	No	-	-
2021-07-15	30.6			
2021-07-16	27.5			
2022-06-26	29.7			
2022-06-27	30.4			
2022-06-28	32.3			
2022-06-29	29.7	2x Yes	No/No	No/Yes
2022-06-30	29.2			
2022-07-01	30.2			
2022-07-02	31.8			
2022-08-14	27.3			
2022-08-15	30.8			
2022-08-16	31.9	2x Yes	Yes/Yes	No/Yes
2022-08-17	28.8			
2022-08-18	32.1			
2022-08-19	32.9			
2022-08-20	27.7			
2024-05-27	28.5			
2024-05-28	28.1	No	-	-
2024-05-29	29.3			

Annex 4. Spectral indices and land surface temperature

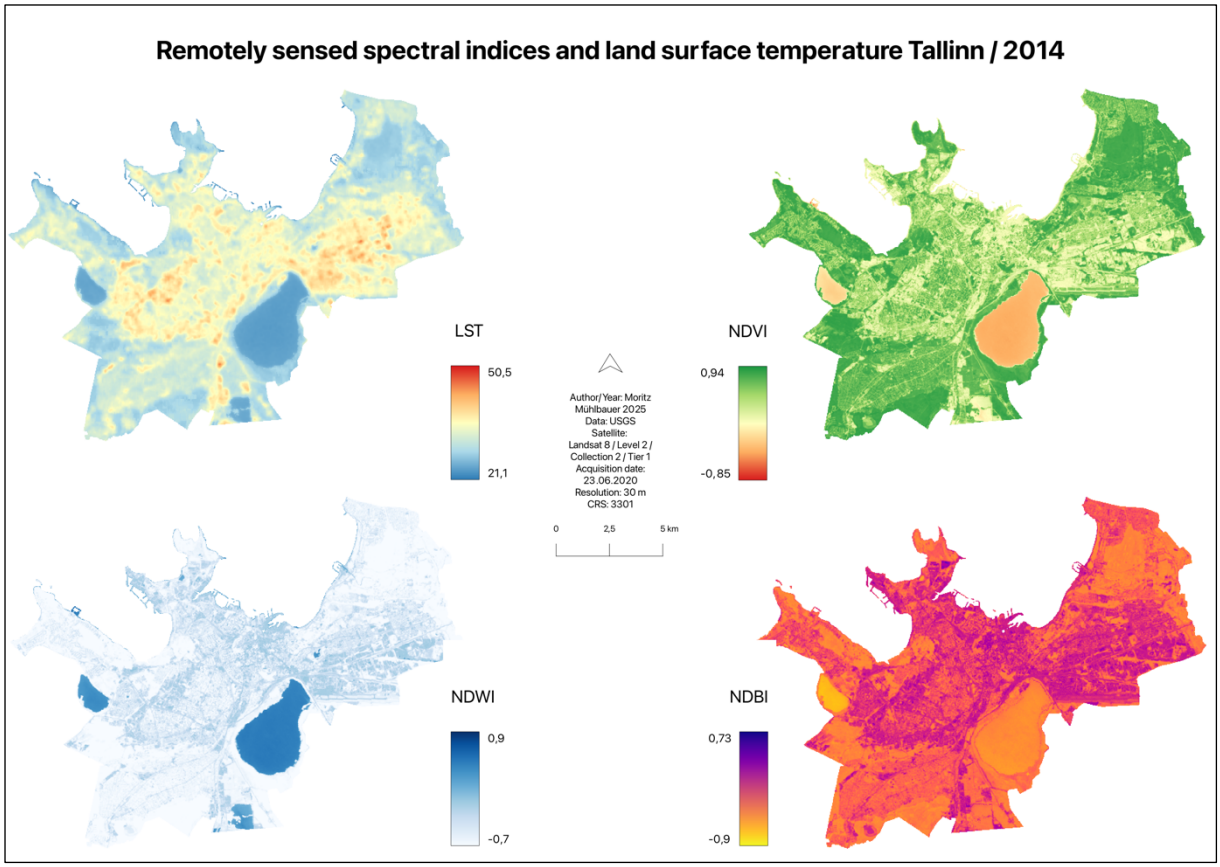

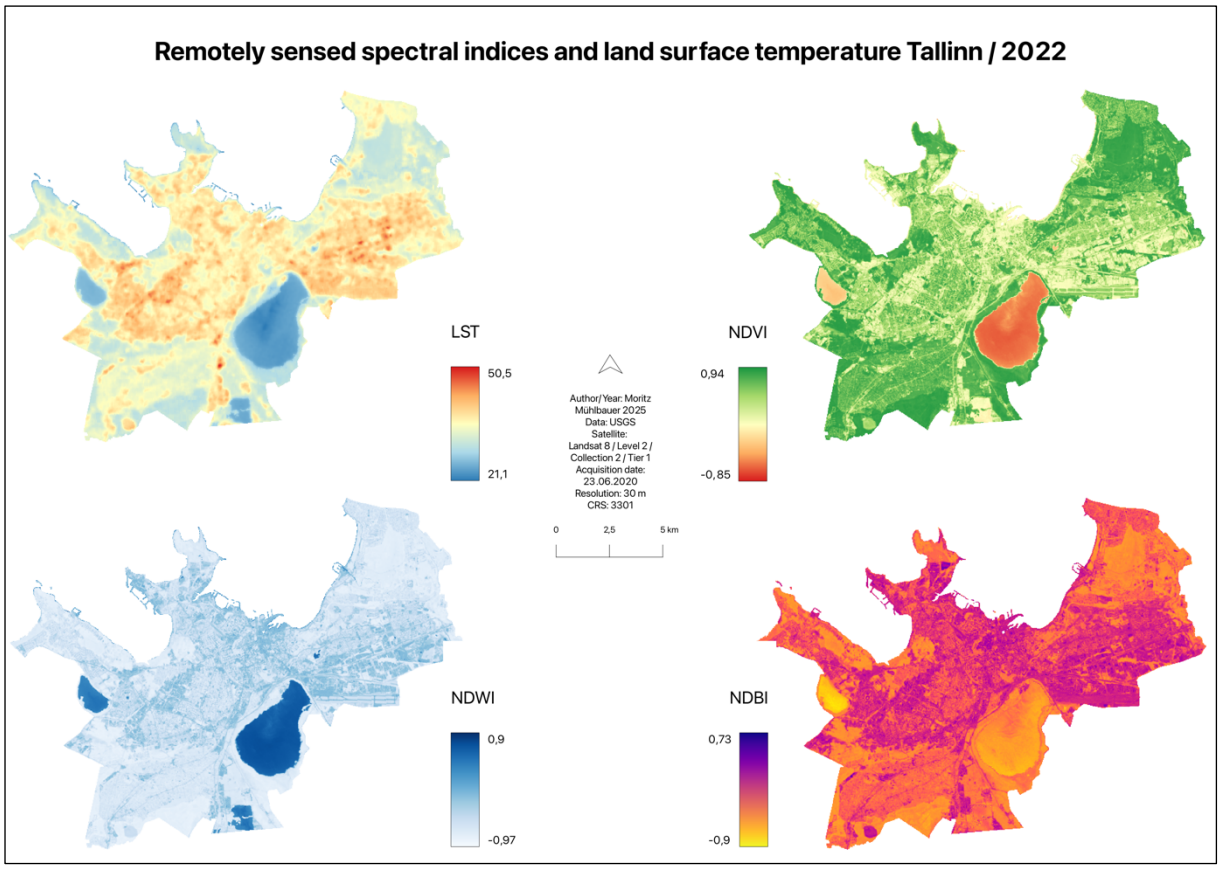

Annex 5. Dominant landcover

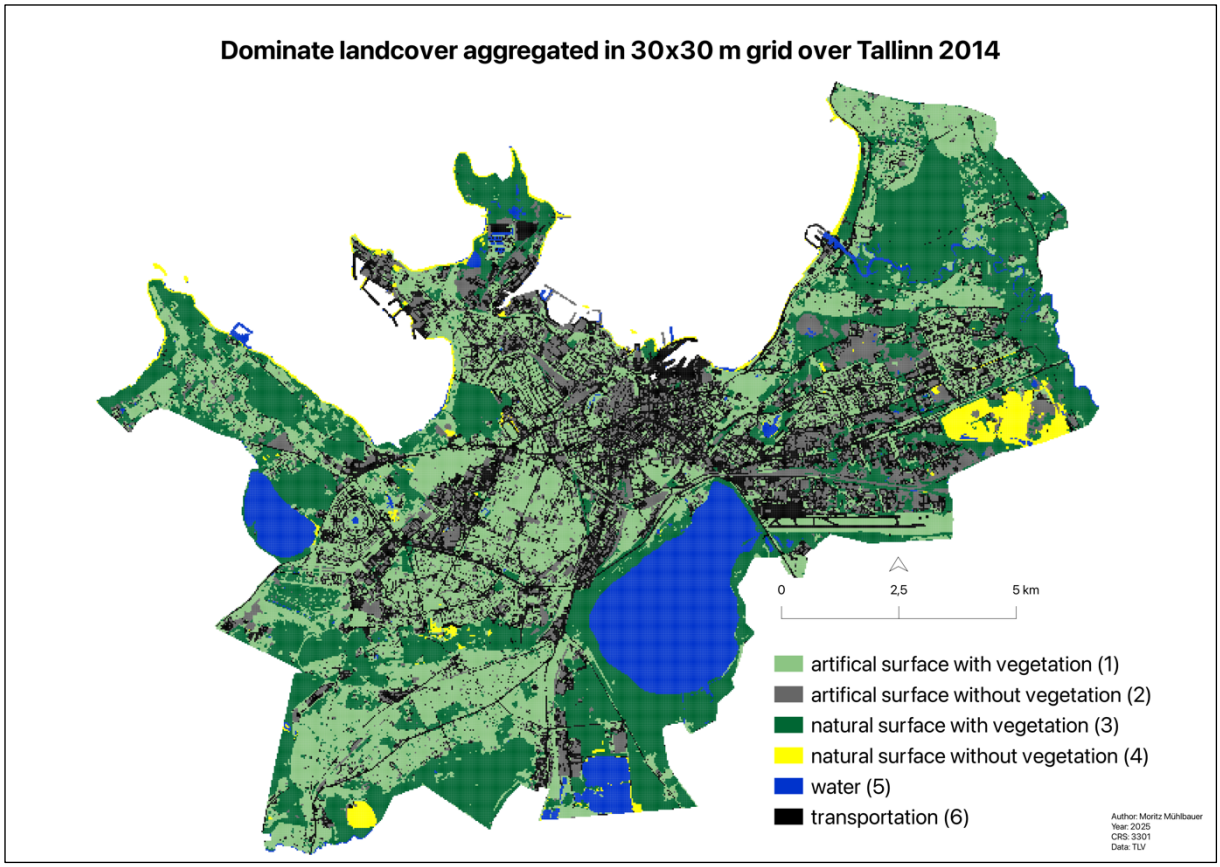

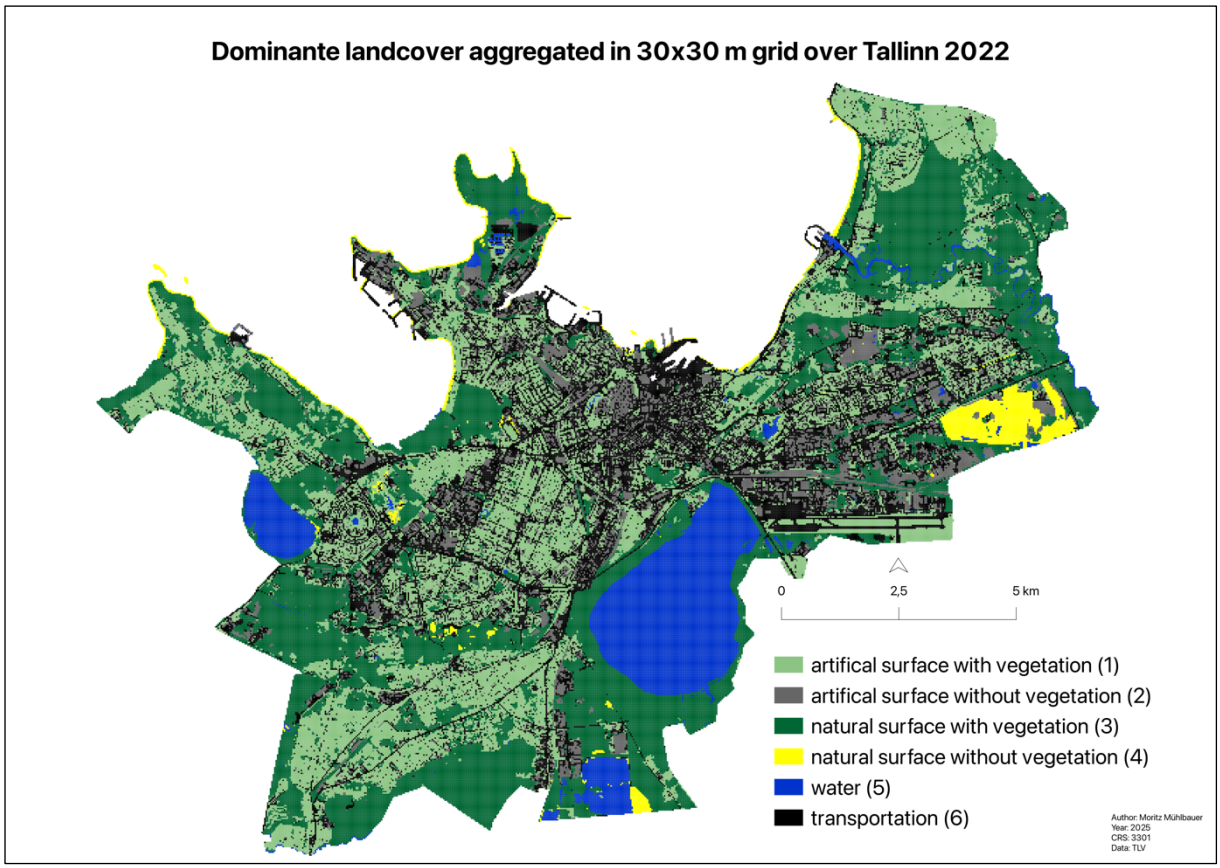

Annex 6. Artificial and natural areas with spectral indices combined

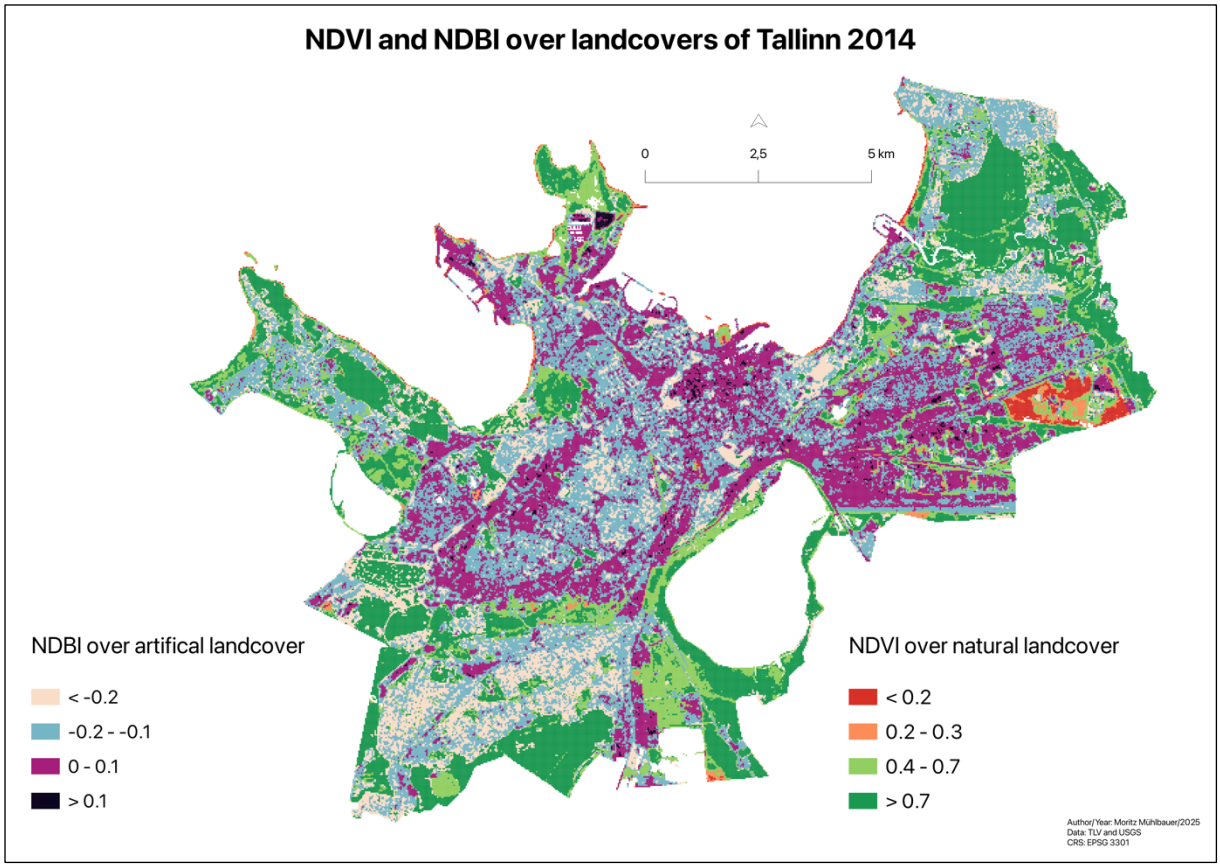

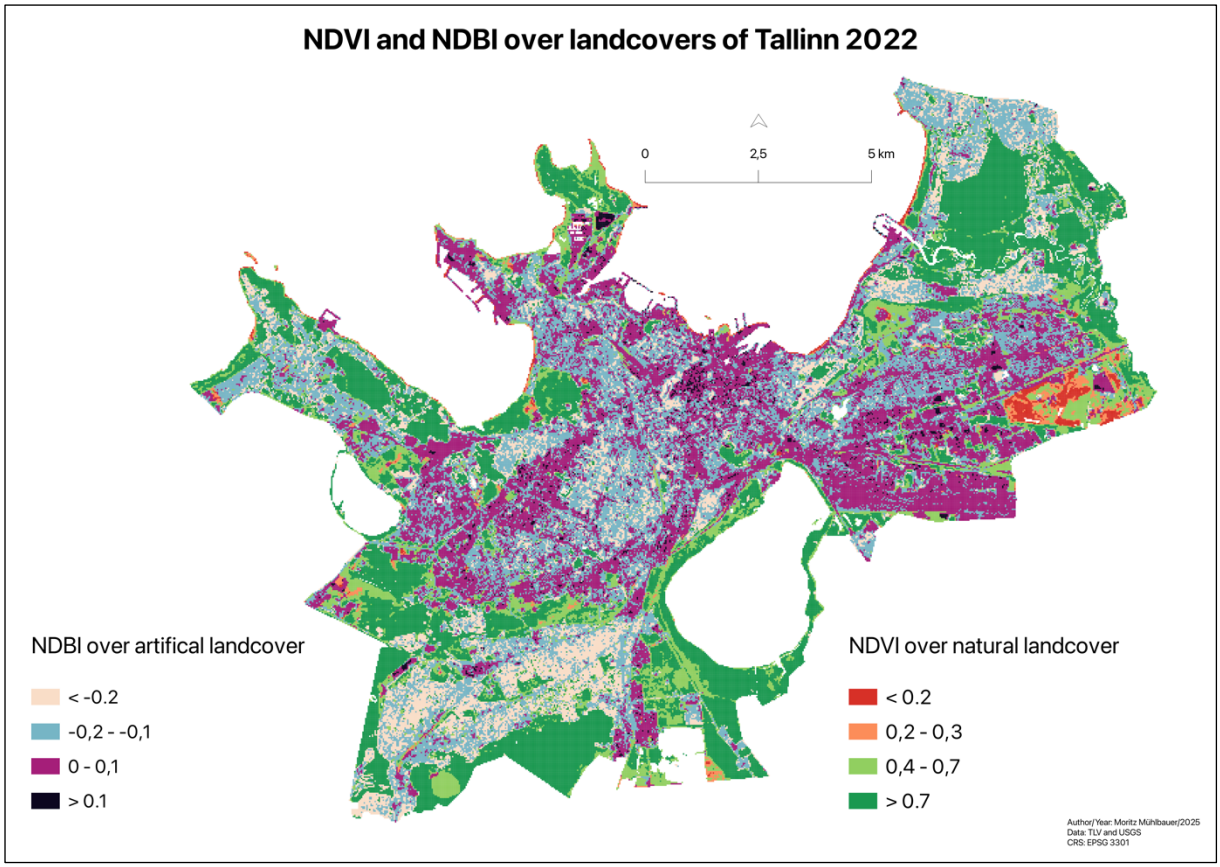

Annex 7. Mean building height

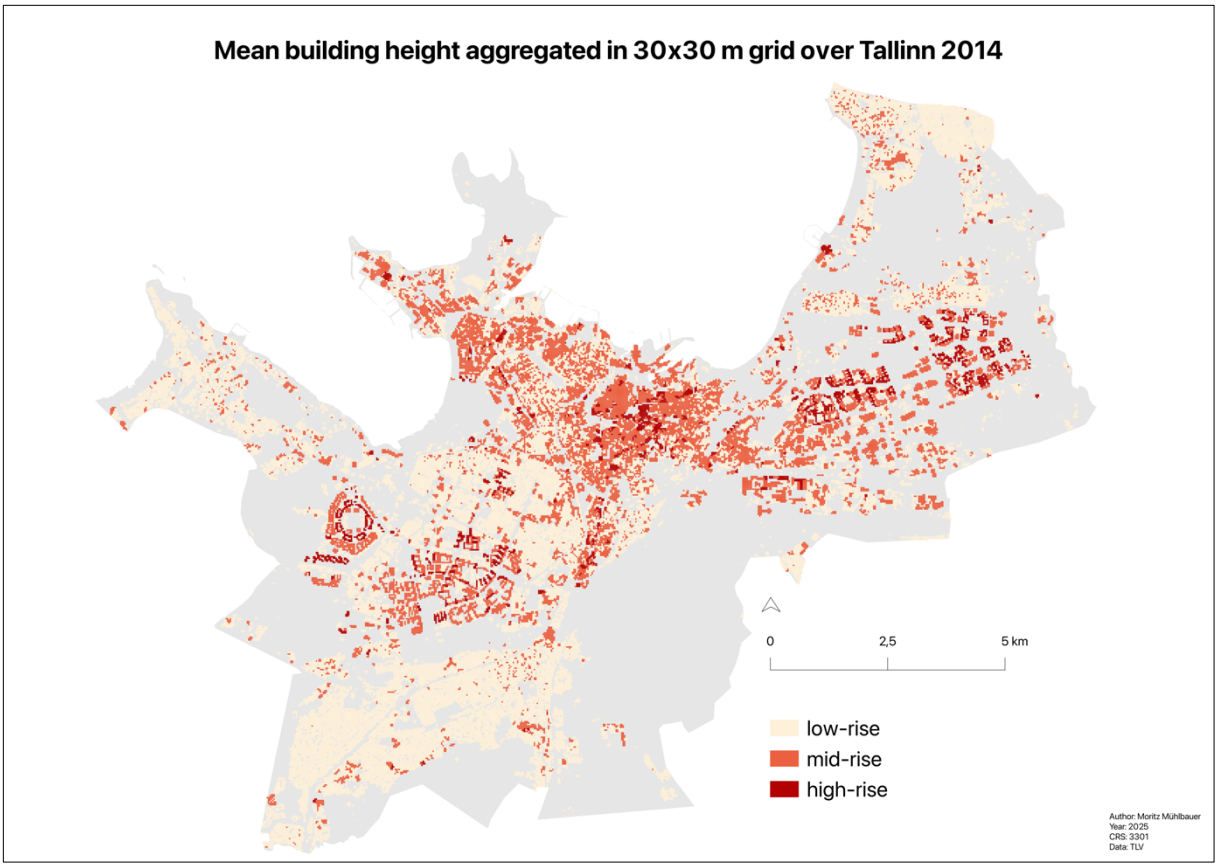

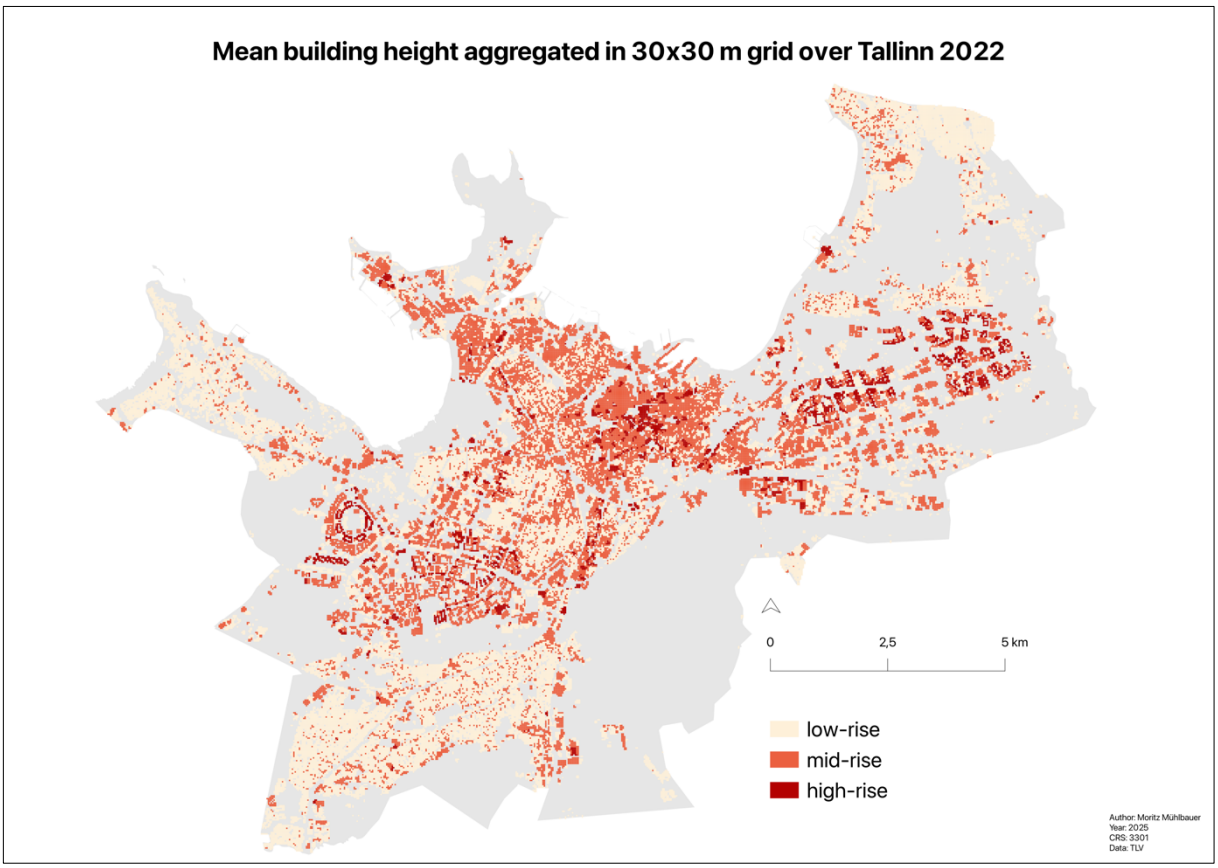

Annex 8. Built fraction

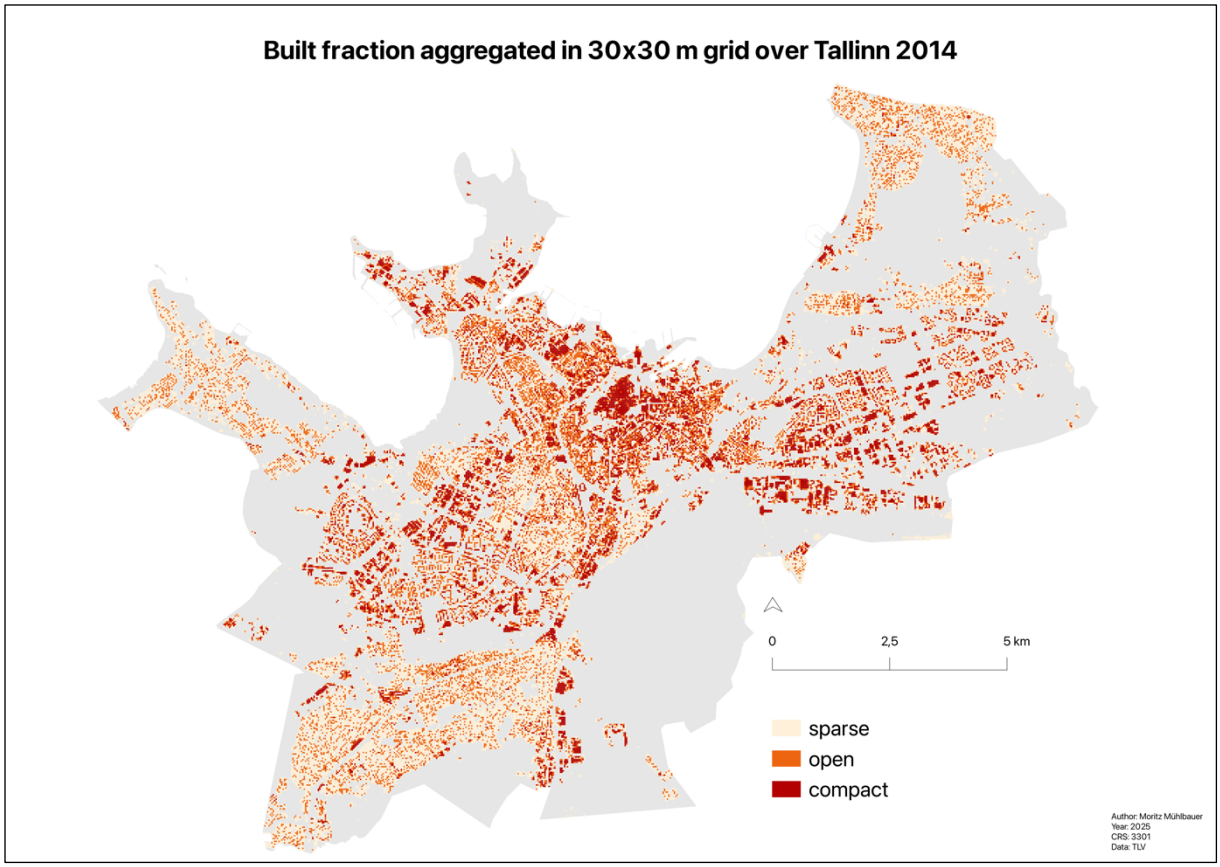

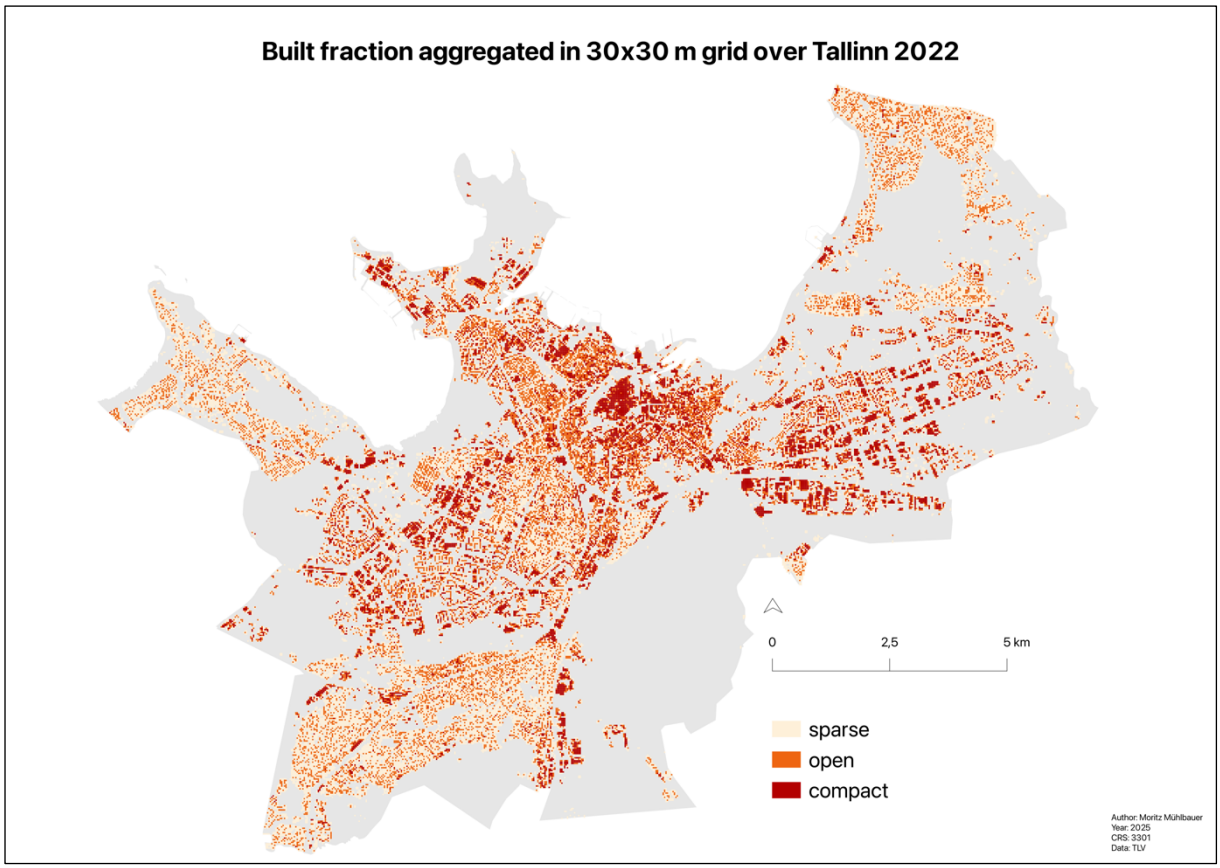

Annex 9. Local Climate Zone classification accuracies

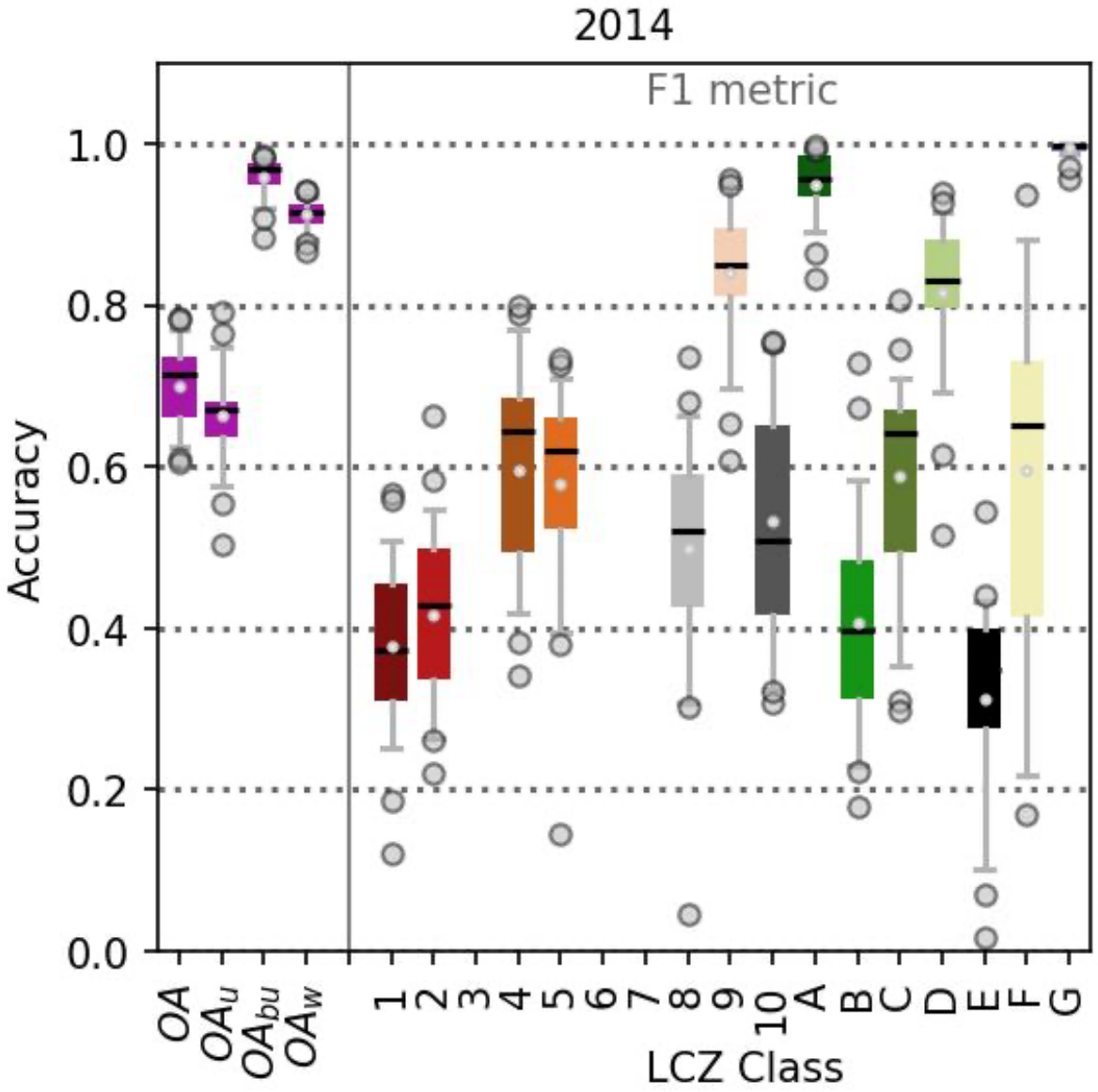

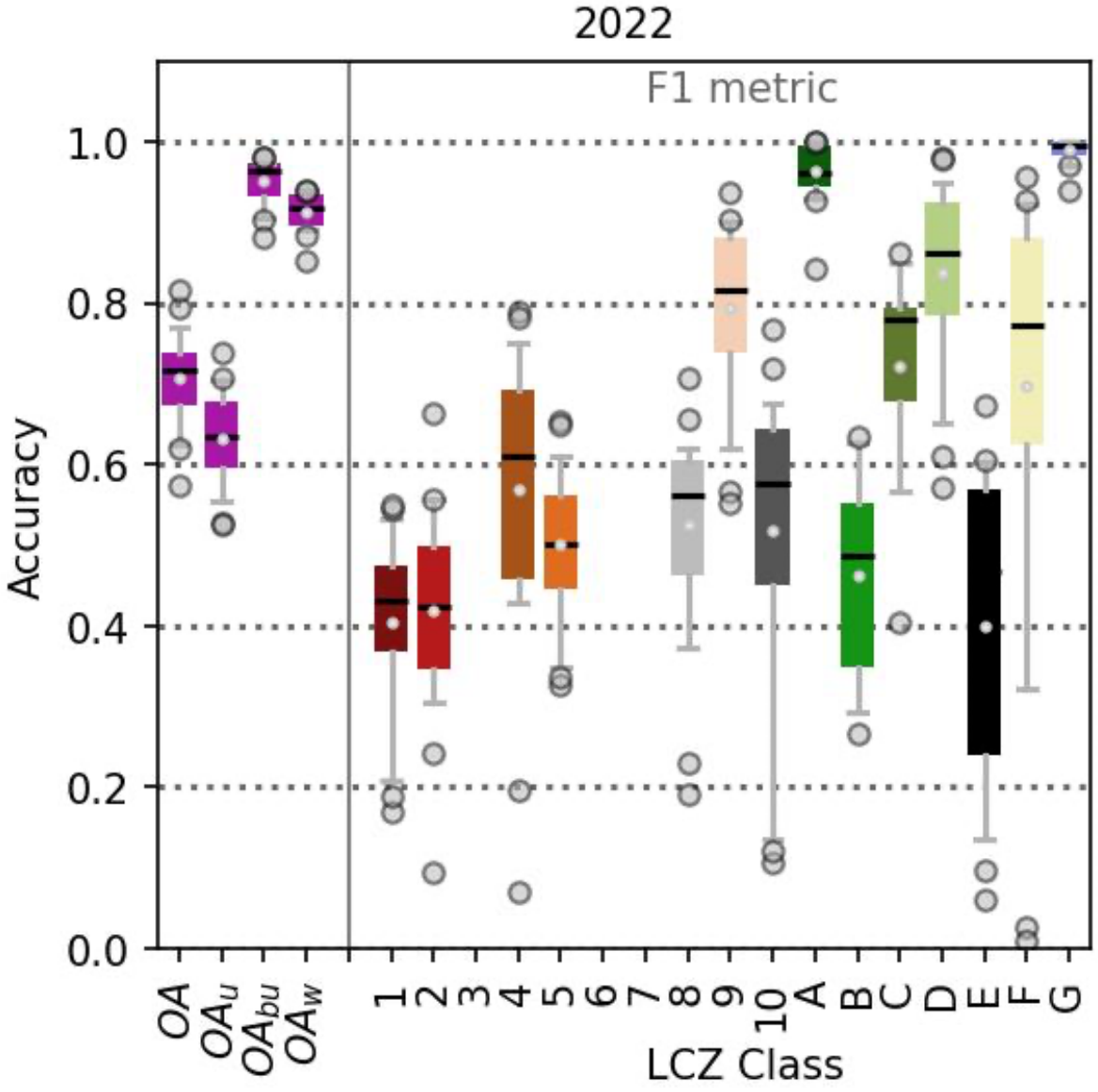
2022
F1 metric
Accuracy
1.0
0.8
0.6
0.4
0.2
0.0
OA
OA_u
OA_bu
OA_w
1
2
3
4
5
6
7
8
9
10
A
B
C
D
E
F
G
LCZ Class

Non-exclusive licence to reproduce the thesis and make the thesis public

1, Moritz Mühlbauer,

grant the University of Tartu a free permit (non-exclusive licence) to

reproduce, for the purpose of preservation, including for adding to the DSpace digital archives until the expiry of the term of copyright, my thesis,

Mapping Surface Urban Heat Islands and the influence of urbanization and heatwaves on urban climate through Local Climate Zones in Tallinn - 2014 and 2022

supervised by Dr. Valentina Sargris

2. I grant the University of Tartu a permit to make the thesis specified in point 1 available to the public via the web environment of the University of Tartu, including via the DSpace digital archives, under the Creative Commons licence CC BY NC ND 4.0, which allows, by giving appropriate credit to the author, to reproduce, distribute the work and communicate it to the public, and prohibits the creation of derivative works and any commercial use of the work until the expiry of the term of copyright.

3. I am aware of the fact that the author retains the rights specified in points 1 and 2.

4. I confirm that granting the non-exclusive licence does not infringe other persons' intellectual property rights or rights arising from the personal data protection legislation.

Moritz Mühlbauer

26/05/2025